Physics of the Earth and Planetary Interiors 351 (2024) 107178

Contents lists available at ScienceDirect

Physics of the Earth and Planetary Interiors

journal homepage: www.elsevier.com/locate/pepi

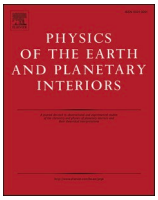

Lateral and radial viscosity structure beneath Fennoscandia inferred from seismic and magnetotelluric observations

Florence D.C. Ramirez [a,b,c,*], Kate Selway [a,b,d], Clinton P. Conrad [a,c], Valerie Maupin [a,c], Maxim Smirnov [e]

[a] Centre for Earth Evolution and Dynamics, University of Oslo, Norway
[b] Department of Earth and Environmental Sciences, Macquarie University, Australia
[c] Centre for Planetary Habitability, University of Oslo, Norway
[d] School of Natural Sciences, University of Tasmania, Australia
[e] Department of Community Planning and Natural Resources, Luleå University of Technology, Sweden

ARTICLE INFO

Keywords:
Upper mantle viscosity
Seismic and magnetotelluric observations
Rock composition and grain size
Glacial isostatic adjustment
Viscosity variations in Fennoscandia

ABSTRACT

Fennoscandia is continuously uplifting in response to past deglaciation, termed glacial isostatic adjustment or GIA, and its mantle viscosity is well constrained from ice sheet and sea level data. Here, we compare those GIA-constrained viscosities for the Fennoscandian upper mantle with geophysically-constrained viscosities. We construct the upper mantle viscosity structure of Fennoscandia by inferring temperature and water content from seismic and magnetotelluric (MT) data. Using a 1-D MT model for Fennoscandian cratons together with a global seismic model, we infer an upper mantle viscosity (below 250 km) of $\sim 10^{21\pm2}$ Pa·s, which encompasses the GIA-constrained viscosities of $10^{20} - 10^{21}$ Pa·s. The GIA viscosities are better matched if the Fennoscandian upper mantle is a wet harzburgite or a dry pyrolite, where pyrolite is ~10 times more viscous than harzburgite. Using the average temperatures and water contents for harzburgitic upper mantle, the GIA viscosities require 1–4 mm grain sizes indicating a diffusion creep regime. In northwestern Fennoscandia, where a high-resolution 2-D resistivity model is available, greater inferred mantle water content implies viscosities that are 10–100 times lower than those for the Fennoscandian Craton. Our work suggests that the combination of seismic and MT observations can improve upper mantle viscosity estimates, especially for regions with laterally-varying viscosity structures or where GIA constraints are not available. Although our method represents an important step forward, viscosity uncertainty can be further reduced by incorporating additional constraints on rock composition, grain size and mantle stress, as well as more accurate geophysical data, into the viscosity calculation.

1. Introduction

Fennoscandia, the northwestern part of the Precambrian East European Craton (see e.g., Bogdanova et al., 1996; Mints et al., 2020 for more details), is continuously uplifting in response to past deglaciation through the process of glacial isostatic adjustment (GIA, e.g., Milne et al., 2001; Lidberg et al., 2007). The observed surface uplift rates measured by geodesy are fastest around central Sweden and the Gulf of Bothnia, which was the position of the maximum ice load during the last glacial maximum (~21 ka), and decrease away from this region (e.g., Vestøl et al., 2019). Such uplift patterns can be predicted by GIA models, which take as input an ice and ocean loading history as well as a model for Earth's interior structure and rheology, which can vary both laterally and radially. The Earth deformation computed from the GIA model predicts patterns of surface uplift and subsidence, as well as horizontal motions, lithospheric stresses, and temporal changes in Earth's gravity, geoid and rotation, all of which can be compared to Earth observations (Whitehouse, 2018). In this way, geodetically-constrained velocity fields like those in Fennoscandia (including horizontal crustal motion) place constraints on the inputs to the GIA model: either the ice load history or Earth's viscoelastic structure (e.g., Milne et al., 2001; Steffen and Kaufmann, 2005; Hill et al., 2010; Kierulf et al., 2014). However, geodynamic processes, such as tectonic deformation, can also affect observed velocities (e.g., Marotta et al., 2004). There is therefore a need for a robust technique to extract GIA-related velocity fields (e.g., Johansson et al., 2002; Lidberg et al., 2007; Hill et al., 2010; Kierulf

* Corresponding author at: Centre for Planetary Habitability, University of Oslo, Norway.
E-mail address: f.d.c.ramirez@geo.uio.no (F.D.C. Ramirez).

https://doi.org/10.1016/j.pepi.2024.107178
Received 8 June 2023; Received in revised form 23 February 2024; Accepted 16 March 2024
Available online 18 March 2024

et al., 2014) from the total velocity fields measured with geodetic data.

Deformation predicted by GIA models includes uncertainties associated with uncertain ice-load history (e.g., Stroeven et al., 2016), sediment loads (e.g., van der Wal and Ijpelaar, 2017), and Earth structure (including lithospheric thickness, density, elastic and viscous structures). This uncertainty could be reduced if these inputs to GIA models could be better constrained. Here we consider Earth's heterogeneous viscosity structure, which is difficult to constrain and is commonly estimated from laboratory-derived flow laws or from surface deformations related to geodynamic processes, such as GIA. Where changes in surface load and the consequent changes in surface elevation can be estimated, the Earth's viscoelastic structure can be calculated, usually in the form of a radial 1-D Earth model with the lithosphere, upper mantle and lower mantle as main layers. However, different lithospheric thicknesses result in different upper mantle viscosities (e.g., Steffen and Wu, 2011), which add uncertainty into GIA-constrained viscosity models. Indeed, seismic tomography models show that lithospheric thickness varies across Fennoscandia (e.g., Calcagnile, 1982; Mauerberger et al., 2022), indicating the existence of lateral heterogeneities that are difficult to implement in a simple Earth model and instead require a robust 3-D Earth model (e.g., Steffen et al., 2006; Kaufmann and Wu, 2002a; Whitehouse et al., 2006; Austermann et al., 2021; Weerdesteijn et al., 2023). Although mantle viscosities calculated from GIA can be used to constrain lithospheric thickness, reported values are different for different GIA models because of differences in the quality and type of GIA data used, and different choices for free parameters used in the modeling.

Since Haskell (1935) estimated the mantle viscosity at 10^{21} Pa·s using decay times of relative sea level (RSL) profiles in Scandinavia, Fennoscandia has been a well-studied region for GIA and its associated viscoelastic structure because of numerous datasets and field observations (e.g., Forte and Mitrovica, 1996; Lambeck et al., 1998a; Milne et al., 2001; Steffen and Kaufmann, 2005; Steffen et al., 2010). Despite the above-mentioned uncertainties, constraining viscosity for Fennoscandia using GIA data, such as sea level and geodetic data, results in a radial viscosity profile with an upper mantle viscosity around $(4-10)\times 10^{20}$ Pa·s beneath ~120 km thick lithosphere (e.g., Forte and Mitrovica, 1996; Milne et al., 2001; Steffen and Kaufmann, 2005). Although sea-level data for Fennoscandia are well-documented (e.g., Lambeck et al., 1998a, 1998b, 2010; Rosentau et al., 2021; Creel et al., 2022) and robust geodetic data are available, such depth-insensitive constraints still limit our ability to constrain any viscosity variations (e.g., Paulson et al., 2005; Kaufmann and Wu, 2002b). Thus, in this study, we aim to constrain the Fennoscandian upper mantle viscosity structure and its lateral heterogeneities using geophysical observations that are independent of any GIA data. We will compare these viscosity predictions to GIA-constrained viscosities (e.g., Forte and Mitrovica, 1996; Steffen and Kaufmann, 2005). From this comparison, we assess the utility and limitations of geophysically-based methods to constrain mantle viscosity before applying these methods to regions without or with limited GIA constraints, such as Greenland and Antarctica.

To constrain mantle viscosity and its lateral heterogeneities, we use seismic and magnetotelluric (MT) data, which constrain lateral and radial variations in mantle parameters that are related to viscosity (e.g., Schotman et al., 2009; Barnhoorn et al., 2011; O'Donnell et al., 2017; Ramirez et al., 2022). By following the method of Ramirez et al. (2022), we infer thermal structures and water content distributions in the Fennoscandian upper mantle from seismic and MT observations and integrate them into Newtonian and non-Newtonian olivine flow laws (e.g., Hirth and Kohlstedt, 2003) to estimate mantle viscosity. From this, we may address the open question of whether a low-viscosity asthenosphere is present (e.g., Fjeldskaar, 1997; Schotman et al., 2009) or absent (e.g., Milne et al., 2004; Steffen and Kaufmann, 2005) beneath Fennoscandia. We also investigate the effect of bulk composition and attempt to determine whether the upper mantle of Fennoscandia is dry (Dixon et al., 2004) or wet (e.g., Kukkonen et al., 2003; Barnhoorn et al., 2011) using the available MT data.

2. Methodology

2.1. Geophysically-constrained viscosity calculation

We employ the method of Ramirez et al. (2022) where (i) temperature is inferred from seismic data using mineralogical models derived from HeFESTo (Stixrude and Lithgow-Bertelloni, 2005, 2011), (ii) water content is constrained from available MT observations using MATE (Özaydin and Selway, 2020), and, where relevant, the results tighten the seismic temperature calculation, and then (iii) the viscosity structure is constructed using the inferred thermal structure and water content distributions (e.g., Hirth and Kohlstedt, 2003).

The thermodynamic model HeFESTo is used to estimate seismic velocities, particularly the shear wave velocity v_S, for a given bulk composition and a range of pressure and temperature values. We have assumed three rock compositions that are geologically common representatives for the upper mantle: pure olivine, harzburgite and pyrolite. Using the global Q model of Romanowicz (1995), we adjust the modelled v_S values with the dispersion due to attenuation so that they can be directly compared to those published in seismic tomographic models. The observed v_S values at different depths or pressures obtained from seismic tomography are then converted to temperature by performing a grid search in a pressure-temperature space for HeFESTo-modelled v_S values for a certain bulk composition. The conversion of seismic velocity to temperature at a given depth or pressure using HeFESTo assumes that all grains are randomly oriented. So, care should be taken when interpreting numerical results from our conversion, particularly when seismic anisotropy is significant. The seismically-inferred temperatures and the corresponding modal mineralogies are used as inputs in the MATE software to calculate the water contents associated with the modelled electrical resistivities from MT data. We utilize the unified olivine conductivity model of Gardés et al. (2014) and other model choices detailed in Ramirez et al. (2022) to calculate bulk electrical resistivities. Since we use olivine flow laws, we extract the water content in olivine for further analysis.

For the viscosity calculation, we employ olivine flow laws, as presented in Hirth and Kohlstedt (2003). Here, we defined the effective viscosity for the mantle as:

$$\eta_{\text{eff}} = \frac{\tau}{\dot{\varepsilon}_{\text{diff}} + \dot{\varepsilon}_{\text{disl}} + \dot{\varepsilon}_{\text{disGBS}}} \tag{1}$$

where τ is differential stress, and $\dot{\varepsilon}_{\text{diff}} + \dot{\varepsilon}_{\text{disl}} + \dot{\varepsilon}_{\text{disGBS}}$ is the total strain rate contributed by diffusion creep, dislocation creep and dislocation-accommodated grain boundary sliding, respectively. The strain rate – stress relationship for each deformation mechanism i is described by,

$$\dot{\varepsilon}_i = A_i \tau^{n_i} d^{-p_i} C_{\text{OH}}^{r_i} exp(\alpha_i \phi) exp\left(-\frac{E_i^* + PV_i^*}{RT}\right) \tag{2}$$

and is controlled mainly by temperature T, water content C_{OH}, grain size d, melt fraction φ, differential stress τ, and pressure P. The pre-exponential factor A, activation energy E^*, activation volume V^*, stress exponent n, grain size exponent p, water content exponent r, and melt factor α are laboratory-derived for each deformation mechanism. Thus, each deformation mechanism has different sensitivities to mantle parameters.

We assume that the upper mantle beneath Fennoscandia is melt-free, in agreement with retrieved xenolith samples (Kukkonen and Peltonen, 1999). The different bulk compositions (pure olivine, harzburgite and pyrolite) are expected to affect seismic velocity and electrical conductivity observations, and therefore the inferred temperature and water contents. In calculating upper mantle viscosity using Eqs. (1) and (2), we consider 1–10 mm grain-sizes as suggested from the xenolith data collected in Finland (Kukkonen and Peltonen, 1999) and garnet

peridotites from Norway (e.g., Cordellier et al., 1981) and assume that upper mantle rocks are under 1 MPa differential stress as computed from a 3-D finite element model for GIA (Barnhoorn et al., 2011). When using seismic constraints only in estimating viscosity, we assume dry to water-saturated conditions at every depth, where water saturation is calculated using the Padrón-Navarta and Hermann (2017) formulation (e.g., Fig. 1).

2.2. Seismic models as constraints

In this study, we mainly use the global shear wave velocity model of Schaeffer and Lebedev (2013) due to its usefulness in providing geological interpretations and structures consistent with other observational constraints (e.g., Klöcking et al., 2018; Davies et al., 2019; Ball et al., 2021) and good resolution at sub-lithospheric depths. The global seismic model shows lateral variations in shear wave velocity across Fennoscandia (e.g., $\Delta v_{SV} \sim$ 0.27 km/s at 190 km depth; Fig. 1a), which can be translated into variations in temperature ($\Delta T \sim$ 600 K, Fig. 1 middle panel), and so into viscosity (e.g., $\Delta\eta \sim 10^8 - 10^{10}$ for dry conditions, Fig. 1 right panel). These variations in temperature and viscosity differ for different bulk compositions. Calculations made assuming a pure olivine composition result in temperatures that are ~100 K lower than those assuming a peridotitic composition (harzburgite and pyrolite), and therefore lead to higher viscosities (by factors of 10 – 1000, compare Figs. 1c and 1d to the rest of Fig. 1, right panel). In contrast, harzburgite and pyrolite have similar lateral distributions of temperature and viscosity, with pyrolite typically ~ 30 K hotter (Figs. 1e and 1h), and less viscous by a factor of 2 – 10 (e.g., Fig. 1f/1g vs. Fig. 1i/1j).

From GIA observations, the cratonic interior of Fennoscandia is more viscous than the continental margins or along the western coast (e.g., Steffen et al., 2006; Whitehouse et al., 2006; Kaufmann and Wu, 2002a), which is consistent with our seismically-constrained viscosities for either dry or water-saturated conditions (right panel, Fig. 1). For instance, southern Norway has slower wave speeds compared to the interior of Fennoscandia, which may indicate that it is hotter and less viscous, leading to a faster GIA response to deglaciation (e.g., Weerdesteijn et al., 2022), if we assume that seismic anomalies are purely of thermal origin.

In the remaining part of this paper, we mainly focus on the cratonic interior of Fennoscandia defined by the white polygon in Fig. 2a due to the available MT data (see Section 2.3 for details). We averaged the global seismic model of Schaeffer and Lebedev (2013) for that cratonic domain area (pale blue patch, Fig. 2b), and use that averaged velocity profile for thermal and viscosity calculations. We also use the regional seismic models (also v_{SV}) of Maupin et al. (2022) for Norway-Sweden (pink line, Fig. 2b) and Bruneton et al. (2004) for Finland (turquoise green line) in constraining temperature and viscosity beneath these two areas (Fig. 2a), and compare these results with those for the cratonic domain. The shear wave velocity model for Finland reported in Bruneton et al. (2004) is corrected for Q. Therefore, in order to be consistent with other models that have not been corrected for Q and with our procedure, we calculated the uncorrected velocities (turquoise green, Fig. 2b) following information given in Bruneton et al. (2004).

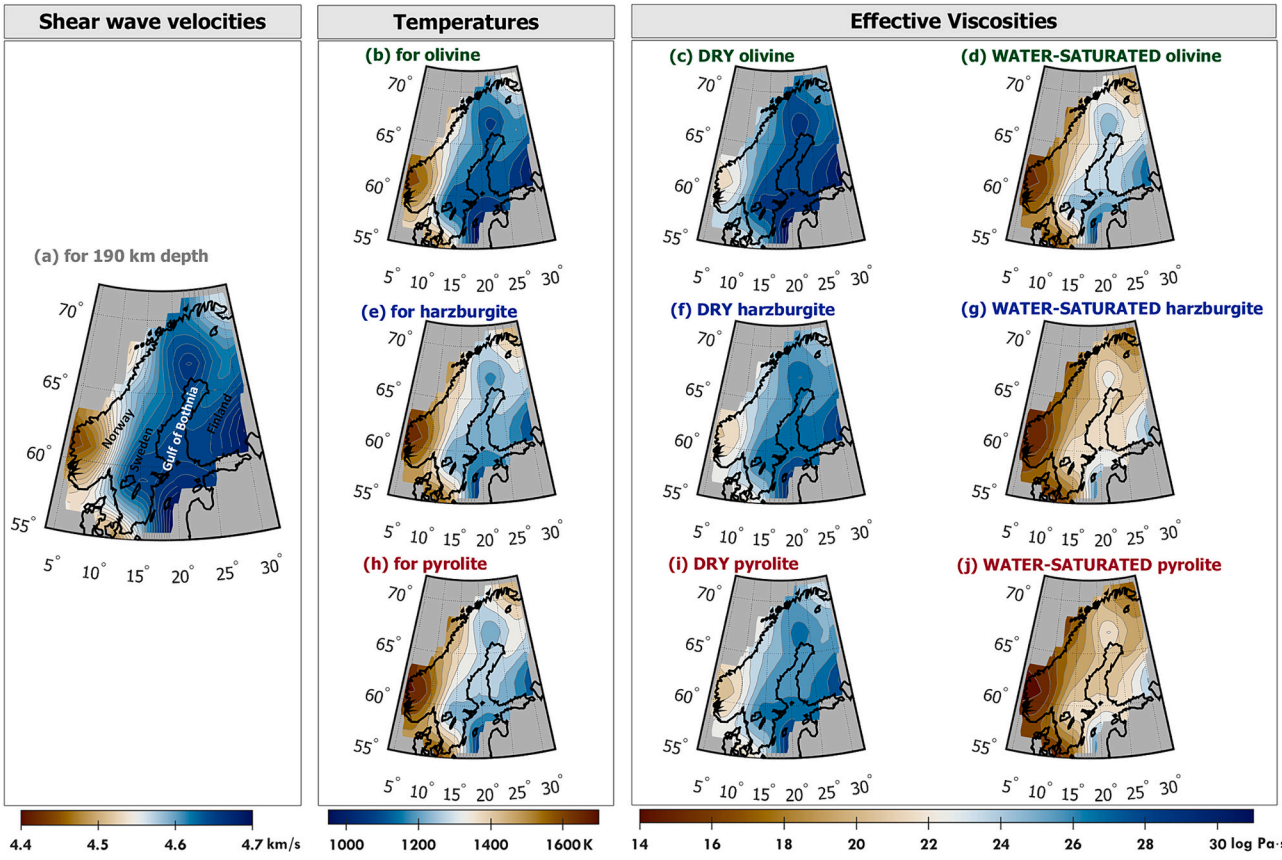

Fig. 1. Inferred lateral variations in temperatures and viscosity at 190 km depth for Fennoscandia from seismic data only. (a) Shear wave velocities are from Schaeffer and Lebedev (2013) for 190 km depth. Different bulk compositions are considered when converting seismic velocity to temperature and calculating effective viscosities: (b-d) olivine, (e-g) harzburgite, and (h-j) pyrolite. Since water content is not constrained by seismic data, we assume dry (0 ppm H/Si) and water-saturated (> 1000 ppm H/Si; Padrón-Navarta and Hermann (2017) formulation) conditions. The effective viscosities are calculated for 10 mm grain size and 1 MPa stress. The contour intervals used are 0.01 km/s for shear wave velocities, 50 K for temperatures, and 1 log Pa·s for viscosities.

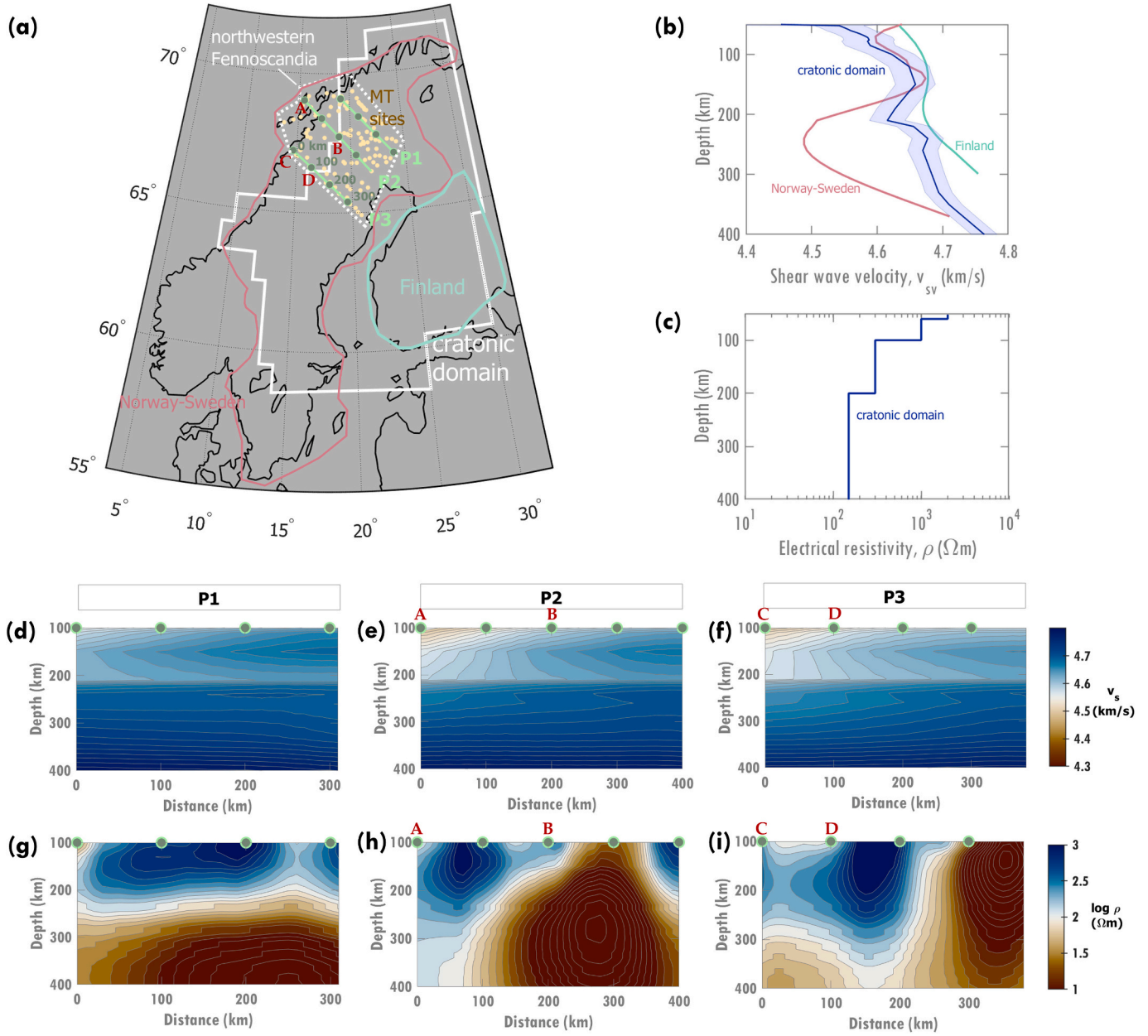

Fig. 2. (a) Different areas across Fennoscandia considered in our viscosity calculation: cratonic domain (solid white polygon), Norway-Sweden (solid pink polygon), Finland (blue green polygon), and straight line profiles (light green lines, labelled P1, P2, and P3) in northwestern Fennoscandia (dotted white polygon) with indicated MT sites (yellow dots) used to constrain 2-D electrical resistivity models (Cherevatova et al., 2015; panels g – i). (b) Shear wave velocities are averaged for the areas indicated in panel (a). The shear wave velocities for the cratonic domain are derived from the global seismic model of Schaeffer and Lebedev (2013), while those for Norway-Sweden and Finland are from regional seismic model of Maupin et al. (2022) and Bruneton et al. (2004), respectively. The shear wave velocity bounds for the cratonic domain (blue patch) are 1σ from the average line. (c) A 1-D electrical resistivity model for the cratonic domain from Varentsov et al. (2002). This resistivity model is also used together with regional seismic models for Norway-Sweden and Finland. The detailed 2-D shear wave velocity (d - f) and electrical resistivity (g – i) profiles for each profile in northwestern Fennoscandia (P1, P2, and P3) have 10 km × 10 km grid size. Points A, B, C and D are indicated here for discussion purposes in Section 3.3. Note that lines AB and CD are not included in the cratonic domain. (For interpretation of the references to colour in this figure legend, the reader is referred to the web version of this article.)

2.3. MT models as constraints

When constraining the water content beneath Fennoscandian cratons (including Norway-Sweden and Finland) using MT data, we are limited to a 1-D electrical resistivity profile (blue solid line, Fig. 2c), which is an average calculated by Varentsov et al. (2002) from different resistivity models obtained mostly in the Fennoscandian cratonic domain (indicated by the white polygon in Fig. 2a). Using the averaged 1-D resistivity profile (Fig. 2c) together with the averaged velocity profiles for the cratonic domain, Norway-Sweden and Finland (Fig. 2b), we can estimate the associated water content and viscosity structure for each area and compare it with GIA-constrained radial viscosity profiles.

Due to data availability, we can only present detailed lateral variations in viscosities using both seismic and MT observations for the northwestern part of Fennoscandia, where 2-D electrical resistivity profiles with good depth resolution down to 400 km are available (Cherevatova et al., 2015). Since the 2-D MT and global seismic models have different lateral resolutions depending on the distributions of sites used in the inversions, we interpolated these models with grid sizes of 10 km × 10 km beneath profiles P1, P2 and P3 (Figs. 2d to 2i; location

shown in Fig. 2a).

3. Constraints on upper mantle viscosity using both seismic and MT observations

We need both seismic and MT data to put tighter bounds on the Fennoscandian upper mantle viscosity. Here we show the utility of the method of Ramirez et al. (2022) by comparing the viscosities estimated from geophysical data with those from GIA. We demonstrate the viscosity estimates when using global (Section 3.1) and regional (Section 3.2) seismic models paired with a 1-D MT model and using 2-D MT models (Section 3.3).

3.1. A 1-D viscosity model for the entire cratonic domain of Fennoscandia

Here we present our inferred temperature, water content and viscosity profiles with associated uncertainties when using seismics only (Figs. 3a – 3d) and when combining seismics and MT (Figs. 3e – 3h). When using only seismic constraints to calculate viscosities, the calculated viscosity structures have large uncertainties (up to $\sim 10^{\pm 4}$ Pa·s in some parts of the model space; Fig. 3d) because water content is unconstrained (Fig. 3b). Apart from temperature and water content, the magnitudes of viscosity also depend on the assumed bulk composition of the upper mantle. A pure olivine upper mantle is colder and more viscous than harzburgite or pyrolite, and shows average viscosity (green line, Fig. 3c) 100–10,000 times higher than GIA-constrained profiles (FM96 and SK05; Forte and Mitrovica, 1996 and Steffen and Kaufmann, 2005). In contrast, the average viscosity profiles for both harzburgite (blue line) and pyrolite (red line) below 250 km are less than a factor of 10 different than the FM96 and SK05 viscosity models. They can match FM96 and SK05 models (10^{20} – 10^{21} Pa·s) if the upper mantle is interpreted to be wet as constrained by seismic and MT models.

When MT data are included into our viscosity estimates (Figs. 3e–3h), the temperatures may or may not be further constrained, depending on the composition and the compatibility of seismic and MT data (Fig. 3e), and the water content distribution is more tightly bounded (Fig. 3f). These constraints significantly reduce the viscosity uncertainty ($\sim 10^{\pm 2}$ Pa·s; Fig. 3h) and improve the fit to GIA-constrained viscosity profiles (FM96 and SK05), particularly between 150 and 250 km. The colder and wetter pure olivine profile is more viscous and has larger viscosity uncertainty than harzburgite and pyrolite (Figs. 3g and 3h). Consistently, the average viscosities for a pure olivine model are larger than the GIA-constrained viscosity models by factors of ~3 – 1000. This implies that pure olivine is not a good representative composition for the upper mantle, as expected. On the other hand, average viscosities assuming pyrolite ($10^{21.1}$ – $10^{22.1}$ Pa·s) and especially harzburgite ($10^{20.4}$ – $10^{21.6}$ Pa·s) are closer to the FM96 and SK05 models (10^{20} – 10^{21} Pa·s), particularly below 250 km. For both compositions, viscosity structures derived from seismic and MT observations match GIA estimates for viscosity, despite a higher water content for harzburgite below 250 km (Fig. 3g). The MT constraints indicate wet conditions between 150 and 250 km (regardless of composition), which strongly supports

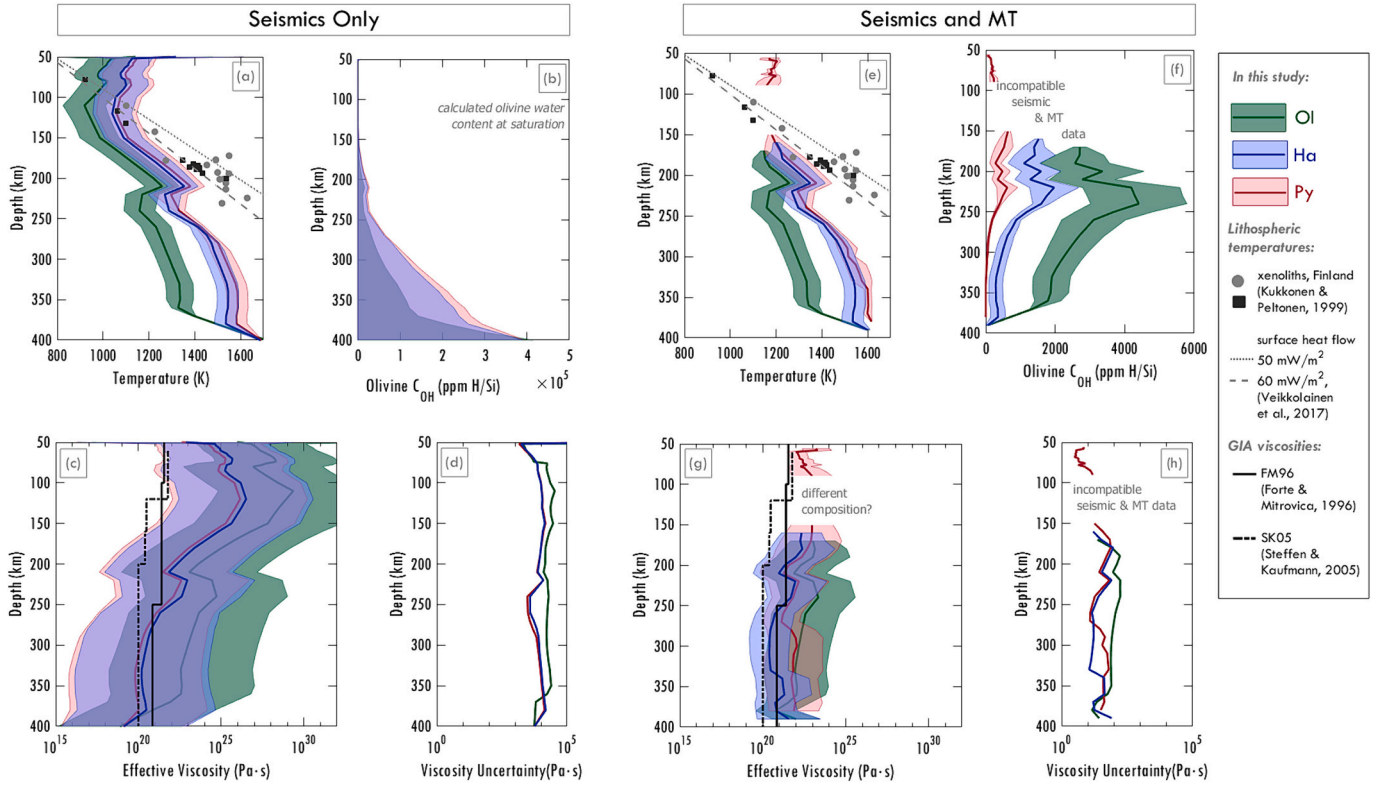

Fig. 3. Inferred temperature and water content, and constructed viscosities from (a-d) seismic, and (e-h) both seismic and MT data for Fennoscandian cratons. (a) The thermal structures for different bulk compositions (Ol = olivine, Ha = harzburgite, Py = pyrolite) are inferred from shear wave velocities for the cratonic domain in Fig. 2b using HeFESTo. Lithospheric temperature estimates from mantle xenoliths using BKN (grey circles) and FB (black squares) thermobarometers (details in Kukkonen and Peltonen, 1999) and from heat flow data for Fennoscandia (dashed and dotted grey lines; Veikkolainen et al., 2017) are shown here for comparison (detailed discussion in Section 4.2). (b) The water content for each composition ranges from 0 ppm H/Si to water-saturation is assumed since water content is not constrained by seismics. The water saturation condition is quantified using the Padrón-Navarta and Hermann (2017) formulation. (c) The constructed effective viscosities are calculated using (a) and (b), with corresponding large viscosity uncertainties (d). When integrating MT data, we obtain better constraints on the temperature (e) and water content (f) profiles, and viscosity structures (g), resulting in reduced viscosity uncertainties (h). The constructed viscosities are calculated for 1–10 mm grain sizes and 1 MPa stress. The FM96 (Forte and Mitrovica, 1996) and SK05 (Steffen and Kaufmann, 2005) viscosity profiles are GIA-constrained.

the conclusion of Kukkonen et al. (2003) that the lithospheric mantle is wet (100–1000 ppm H/Si) based on observations of decrepitated fluid inclusions in mantle xenoliths. Consistently, the SK05 and FM96 models lie on the low end of the viscosity estimates for harzburgite and pyrolite, respectively (Fig. 3g). Between 90 and 170 km depth, there is an incompatibility between the seismic and MT data using our method because the seismically-inferred temperatures cannot produce the relatively low observed electrical resistivities, even for water-saturated conditions (discussion in Section 5.2).

3.2. 1-D viscosity models beneath Finland and Norway-Sweden

For Finland and for Norway-Sweden, two average 1-D shear wave velocity models are available (Fig. 2b; Bruneton et al., 2004; Maupin et al., 2022). Here we compare viscosity estimates based on these regional seismic models with those based on the global seismic model for the cratonic domain (Fig. 4). These different seismic models yield different thermal profiles (Fig. 4a) and different water contents (Fig. 4b) when integrated with the same 1-D MT model (Fig. 2c). The cratonic domain has higher velocities than Norway-Sweden (pink line) but is comparable with Finland (turquoise green line). These high velocities are expected for the cratonic domain because regions in southern Sweden and a portion of northern Norway with relatively low velocities (Fig. 1a) are excluded when we extracted the seismic-depth profile for the cratonic domain from the global seismic model. Consequently, the cratonic domain reflects intermediate temperatures and water contents between those for Norway-Sweden and Finland (Figs. 4a and 4b), indicating that Norway-Sweden may reflect maximum temperature bounds while Finland reflects minimum temperature bounds.

Lithospheric temperatures constrained for Norway-Sweden from the regional seismic models are consistent with those derived from Finland xenoliths (grey dots, Fig. 4), while Finland is interpreted to be colder. However, the deeper seismically inferred Norway-Sweden mantle geotherm seems to be unrealistic since temperature decreases at depths greater than ~250 km instead of following an adiabat. Regional seismic velocity models for sub-lithospheric depths in Maupin et al. (2022) have very large reported uncertainties (i.e., ±0.13 km/s to ±0.32 km/s, which translate into approximately ±350 K to ±900 K). These large velocity uncertainties indicate that the constrained high temperatures for the Norway-Sweden upper mantle are not reliable. Consequently, these unrealistic high mantle temperatures of Norway-Sweden cannot constrain water contents (pink line, Fig. 4b) and viscosities (pink patch, Fig. 4c). The incapability of converting the electrical resistivity model into water content may also be due to the unrealistically high temperatures or may alternatively indicate that the 1-D MT model used in the calculation is not applicable to all Norway-Sweden areas.

The Norway-Sweden region shows a positive radial anisotropy, where v_{SH} waves are faster than v_{SV} by 2% - 3% (Maupin et al., 2022), consistent with other recent regional seismic studies (e.g., Eken et al., 2008; Lebedev et al., 2009; Vinnik et al., 2014). When accounting for this seismic radial anisotropy in our temperature calculation, our inference has improved (yellow lines, Fig. 4). Since HeFESTo assumes isotropic minerals, we estimate the Voigt shear wave velocity as an effective isotropic velocity v_S using the Babuska and Cara (1991) formulation and use this calculated v_S to infer a new temperature. Because of significant radial anisotropy, Voigt v_S is expected to be larger than v_{SV}. Thus, the Voigt v_S translates into lower temperatures than those derived directly from v_{SV} (yellow vs. pink lines, Fig. 4a). This colder geotherm provides better constraints on water content and viscosity in the upper mantle of Norway-Sweden (below 250 km; yellow line, Figs. 4b and 4c), where it is interpreted as dry and its viscosity structure coincides with the cratonic domain.

Seismic velocities for Finland are slightly higher than average velocities for the cratonic domain, resulting in a slightly colder, wetter and more viscous upper mantle (turquoise green vs. blue lines, Fig. 4). As expected, these minimal differences between Finland and the cratonic domain result in an overlapping viscosity structure. We infer a similar viscosity structure for Finland (not shown), still slightly more viscous than for the cratonic domain, when using the Q-corrected velocity profile in Bruneton et al. (2004). Considering the observed radial anisotropy (above 200 km; Pedersen et al., 2006) for Finland lithosphere in our temperature calculation, we expect a decrease in temperature and an increase in water content, and potentially an increase in Finland's lithospheric viscosity as well. This illustrates that using regional seismic models for inferring temperatures is challenging and that the co-location of 1-D averaged seismic and MT models might be a limiting factor.

3.3. 2-D viscosity models beneath northwestern Fennoscandia

To interrogate lateral variations more thoroughly, 2-D models of temperature, water content and viscosity were calculated along three profiles (P1, P2 and P3, Fig. 5) where 2-D MT data are available. These calculations were made using seismic velocities (Schaeffer and Lebedev, 2013) and electrical resistivities at 10 km × 10 km regularly spaced intervals extracted from the original geophysical models (Figs. 2d to 2i), assuming a harzburgite composition, 10 mm grain sizes and 1 MPa

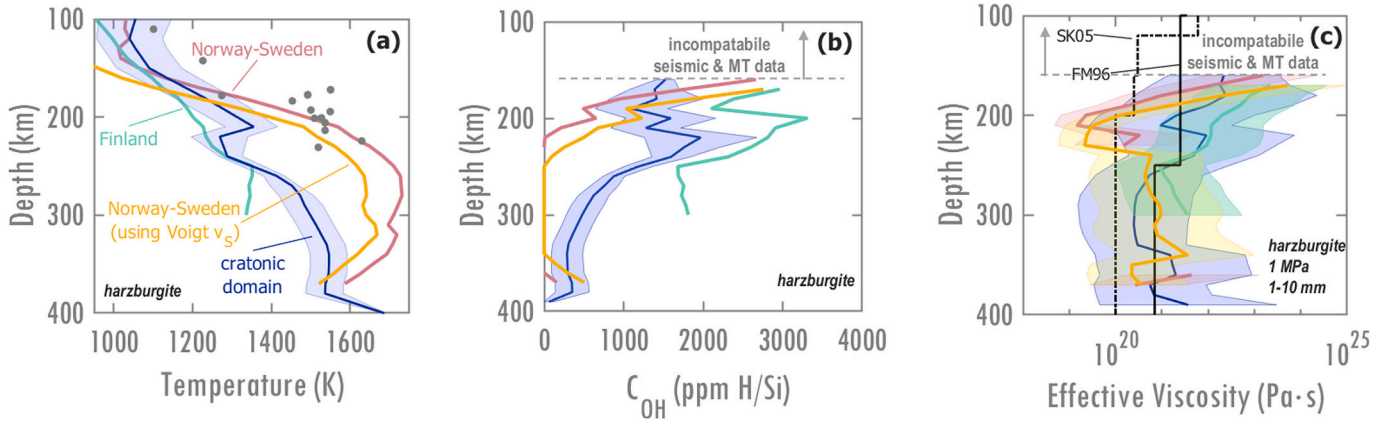

Fig. 4. Constraints from regional versus global seismic models. (a) Temperatures inferred from vertical shear wave velocity models in Fig. 2b for Norway-Sweden (pink line), Finland (green line) and the cratonic domain (blue patch) for a harzburgite composition. The yellow profiles are inferred for Norway-Sweden using Voigt shear wave velocities to account for strong radial anisotropy. The grey data points are xenolith temperatures from Kukkonen and Peltonen (1999). The thermal structures, combined with the 1-D MT model for Fennoscandia (Fig. 2c) result in water content estimates in (b). The temperatures in (a), water contents in (b), a stress of 1 MPa, and 1–10 mm grain sizes produce viscosity structures for harzburgitic upper mantle in (c). As in Fig. 3, FM96 and SK05 are GIA-constrained viscosity profiles. (For interpretation of the references to colour in this figure legend, the reader is referred to the web version of this article.)

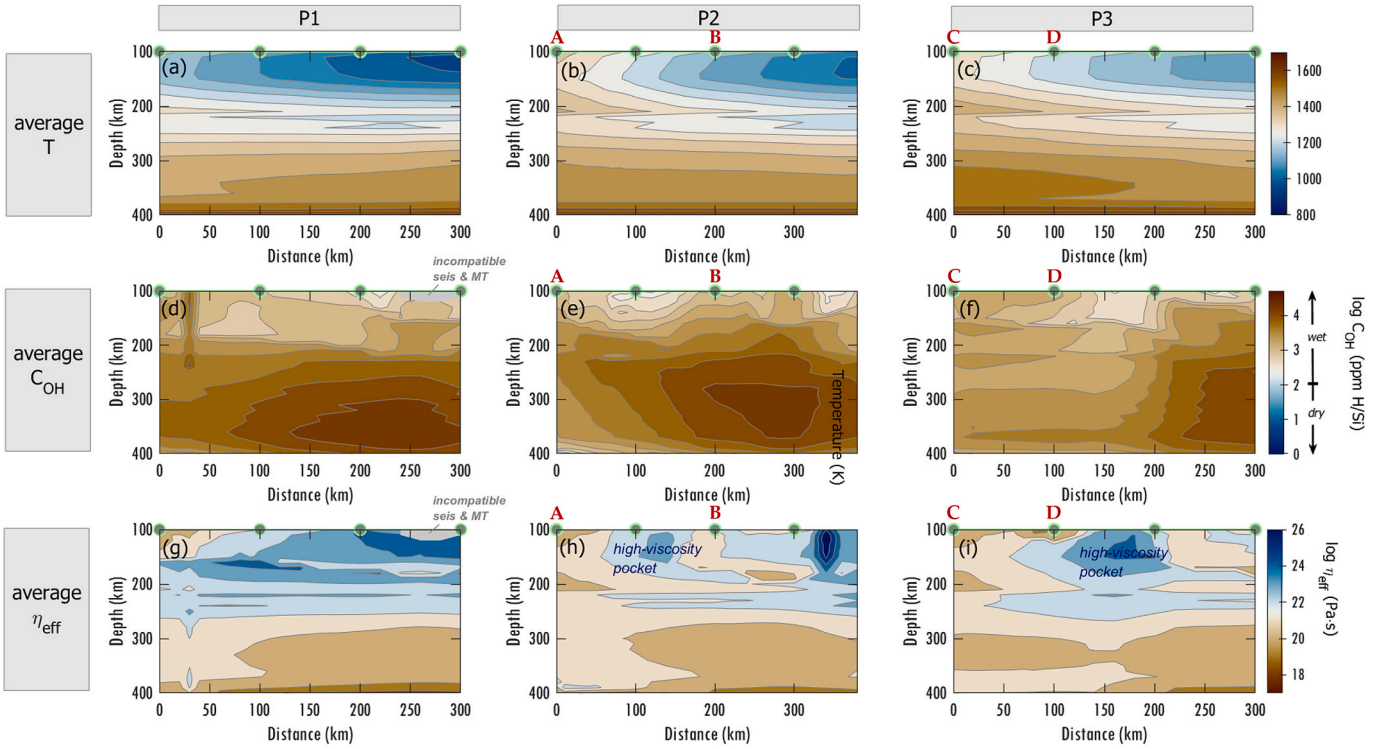

Fig. 5. The 2-D average temperatures (top panels), water contents (middle panels) and viscosities (bottom panels) for each line profile in northwestern Fennoscandia (in Fig. 2a), where all profiles here run from the northwest on the left to the southeast on the right. We infer these 2-D structures by using both seismic (Fig. 2d – 2f) and MT (Fig. 2g – 2i) 2-D models for harzburgite with constant geophysical uncertainties of ±0.05 km/s and ±0.5 log S/m, respectively. These uncertainties translate into temperature, water content and viscosity ranges per depth across each profile, with average values shown here. The small grey patches in the water content and viscosity models for Profile 1 indicate incompatibility between seismic and MT data that results in unconstrained water content, and thus also viscosity. Line profiles A-B and C-D show important results as discussed in Section 3.3.

stress. The observed incompatibility between seismics and MT (Sections 3.1 and 3.2) can be minimized by adding realistic uncertainties into the geophysical models, which provides ranges of temperature and water content that can produce the estimated electrical resistivities. Since uncertainties are not reported for the geophysical models that we used, we assume constant uncertainties of ±0.5 km/s (e.g., Lebedev et al., 2009) and ±0.5 log S/m (e.g., Selway et al., 2019) for shear wave velocity and electrical resistivity, respectively (e.g., Ramirez et al., 2022). We add these uncertainties to every node in the meshes, producing average temperatures (Figs. 5a – 5c), water contents (Figs. 5d – 5f) and viscosities (Figs. 5g – 5i) across each profile. The assumed geophysical uncertainties translate into ~ ±2 log Pa·s uncertainty in the upper mantle viscosity (not shown here).

Our calculations suggest lateral and radial variations in upper mantle viscosity across each 2-D viscosity profile attributed to lateral and radial variations in temperature and water content. Generally, the highly resistive regions in the upper 200 km beneath P1, P2 and P3 (blue regions, Figs. 2g to 2i) have high average effective viscosities of ~10^{22} – 10^{24} Pa·s (blue regions, Figs. 5g – 5i) as controlled by the water content and temperature estimates from seismic and MT models. If the bulk composition is pyrolite, these highly resistive regions are expected to be drier, hotter and more viscous than for a harzburgitic composition. Below 250 km depth, average effective viscosities vary within ~10^{20} – 10^{21} Pa·s, which agree well with the GIA-constrained viscosities.

Interestingly, the coastal area or continental margin of P2 and P3 (from A to B and C to D in Fig. 5), which do not belong to the cratonic domain in Fig. 2a, show lower viscosity (~1019 Pa·s) in the upper 250 km than the cratonic interior (~10^{23} Pa·s; below P1), which is consistent with some GIA studies (e.g., Steffen et al., 2006; Whitehouse et al., 2006; Kaufmann and Wu, 2002a). In addition, a shallow, high-viscosity pocket is present below P2 and P3 as inferred from the MT model, which notably coincides with the observed high seismic velocity Lofoten-Norbotten anomaly from the regional seismic model of Mauerberger et al. (2022). This seismic anomaly suggests a heterogeneity in the lithosphere-asthenosphere boundary depth (Mauerberger et al., 2022), which translates into lateral variations in average viscosity (~10^{19} – 10^{25} Pa·s) in the upper 250 km of northwestern Fennoscandia. Lateral variations in the viscosity of the lithosphere can significantly affect GIA uplift rates, with the GIA response typically accelerated above weak regions (e.g., Weerdesteijn et al., 2022). Incorporating weakened and thin lithosphere into coastal areas may improve the uplift rate predictions of Kierulf et al. (2014, 2021), where uplift observations in northern Fennoscandia are faster than predicted.

4. Discussion

4.1. Limitations and geophysical data

Our calculations assume a melt-free upper mantle and limited, olivine-dominated compositions. The flow laws we have applied only consider an olivine composition (Hirth and Kohlstedt, 2003). Accounting for other phases such as pyroxenes (e.g., Chen et al., 2006) may decrease the overall estimated viscosity due to phase mixing and pinning, which change the deformation mechanism and microstructure (e.g., Bercovici and Skemer, 2017; Hansen and Warren, 2015; Tasaka et al., 2020; Warren and Hirth, 2006; Zhao et al., 2019). Furthermore, we assume a constant stress and a limited range of grain sizes. Laterally-varying stresses would certainly affect our viscosity estimates, while choosing a single grain size would put tighter bounds on the viscosity structure.

The resolution of our viscosity estimates is limited by the lateral and depth resolution of the seismic and MT models that we use. The global

seismic model of Schaeffer and Lebedev (2013) depends on the spacing of the crossing seismic rays in this region, while the 1-D electrical resistivity model represents an average of different resistivity models from mostly cratonic domains across Fennoscandia (details in Varentsov et al. (2002)). The global seismic model has a discontinuity at 210 km (e.g., Fig. 2b) due to the use of reference model AK135 (Kennett et al., 1995). This discontinuity is visible as an abrupt jump to higher velocities in the seismic models and corresponds to jumps to lower temperatures and higher viscosities at 210 km depth in our calculations. Since this discontinuity is likely to be a modeling artefact, the jumps in calculated parameters should not be relied upon. Using a localized 2-D resistivity profile (~10 km resolution) for northwestern Fennoscandia together with the global seismic model provides a more detailed viscosity structure (Fig. 5), but the overall resolution of the resulting viscosity model is controlled by the lower resolution of the global seismic model.

For the conversion from seismic velocities to temperature and composition, the global shear wave seismic model of Schaeffer and Lebedev (2013) uses vertically polarized velocities (v_{SV}), while the velocity models calculated from HeFESTo are isotropic (v_S). This discrepancy adds uncertainty into our temperature and viscosity estimates. If anisotropic textures cause v_{SV} to be greater than v_S, then the actual temperatures may be lower than we have inferred (Fig. 4; Section 3.2).

4.2. Temperature estimates from seismic and MT versus xenoliths and heat flow

We compare our geophysically-inferred temperatures, particularly for the upper 250 km, with other estimates from surface heat flow (Veikkolainen et al., 2017) and xenoliths (Kukkonen and Peltonen, 1999) to assess our results (Figs. 3a and 3e). Steady-state, paleoclimatically corrected temperature estimates for 50 mW/m^2 and 60 mW/m^2 surface heat flow (dotted and dashed grey lines, Figs. 3a and 3e), generally imply hotter temperatures than our seismically-inferred estimates. Instead, the trend passes through the temperature estimates from mantle xenoliths, partly because these same xenoliths are used as constraints for mantle heat flow (Kukkonen and Peltonen, 1999). Since mantle xenoliths studied by Kukkonen and Peltonen (1999) are carried to the surface via kimberlite eruptions, we may expect a chemically and thermally modified lithosphere beneath Finland at the time of eruption (~530 Ma). The associated geotherm may have been hotter, and potentially plume-influenced (Torsvik et al., 2010), compared to a generic cratonic geotherm (e.g., Selway et al., 2014; Hasterok and Chapman, 2011) or cratonic Finland today. This suggests that the xenoliths and their associated geotherm represent an upper temperature bound, and the present-day seismically-derived temperatures are consistent with this. In addition, the temperature estimates for harzburgite and pyrolite compositions are closer to a generic cratonic geotherm (e.g., Hasterok and Chapman, 2011) than for olivine (Fig. 3).

4.3. Incompatibility between seismic and MT models

Seismic and MT data seem to be incompatible between 90 km and 170 km depth (Fig. 3). At these depths, electrical resistivities from the MT models are too low to be explained by the temperatures calculated from the seismic models, assuming the limited range of compositions we use for interpretation. The resolution of highly resistive uppermost mantle is often masked by more conductive overlying crust (e.g., Selway, 2018), so the modelled resistivities may be lower than the actual resistivities. These low modelled resistivities result in higher temperatures than we have inferred from seismic velocities, which may be unusually fast either due to anisotropy as discussed above or due to large grain sizes that produce low attenuation. Thus, a decrease in temperature estimates from MT (by increasing the modelled resistivities) or an increase in temperature estimates from seismic constraints would help in reducing the incompatibility between seismic and MT observations. Although xenoliths suggest relatively high lithospheric temperatures as discussed above, present-day lithosphere may be cooler than at the time of xenolith eruption as inferred from seismic data. This may mean that temperature estimates at those depths are probably not the main cause for the observed incompatibility between geophysical data.

A likely cause for the discrepancy is that conductive phases that we do not include in our interpretations, such as phlogopite, amphibole or partial melt, may be present in the uppermost mantle (e.g., Özaydin et al., 2021; Selway, 2014). Mantle-xenolith samples with hydrous minerals (e.g., southwestern Kaapvaal Craton; e.g., Baptiste et al., 2012) and MT models (e.g., Selway, 2014; Özaydin et al., 2021) show that cratonic lithosphere often contains conductive minerals at these depths. Based on P-wave tomography, Bulut et al. (2022) suggest that Archean northern and northeastern Fennoscandia are compositionally modified, while the central part of Fennoscandia and the areas around Stockholm are not, possibly showing a more fertile composition (e.g., Beyer et al., 2006). A modelled composition containing hydrous minerals, more pyroxene and less olivine (Özaydin et al., 2021) would reduce the incompatibility between the geophysical observations.

4.4. Geophysically-derived viscosity uncertainties

In our calculations, we translate the range of geophysical observations for a region into a range of calculated effective viscosities (Eq. 1) as described by $10^{\overline{log\eta_{\text{eff}}} \pm \Delta log\eta_{\text{eff}}}$ where:

$$\overline{log\eta_{\text{eff}}} = \frac{log\eta_{\text{eff},max} + log\eta_{\text{eff},min}}{2} \tag{3.1}$$

$$\Delta log\eta_{\text{eff}} = \frac{log\eta_{\text{eff},max} - log\eta_{\text{eff},min}}{2} \tag{3.2}$$

and $\eta_{\text{eff},max}$ and $\eta_{\text{eff},min}$ are the maximum and minimum effective viscosities. The associated viscosity uncertainties ($10^{\pm\Delta log\eta_{\text{eff}}}$) that we present here using our method can be attributed to uncertainties in the geophysical inputs (Section 4.4.1), that is, the ranges of shear wave velocity and electrical resistivity, which translate into ranges of temperature and water content (e.g., Fig. 6). Apart from temperature and water content, uncertainties in other viscosity model parameters (Section 4.4.2) such as ranges of grain size and stress, and the resulting dominant deformation mechanism also affect the overall viscosity and the associated uncertainty.

4.4.1. Geophysical uncertainties

The geophysical uncertainties are propagated into the viscosity uncertainty through the inferred temperature and water content ranges. Smaller (or negligible) geophysical uncertainties or ranges would result in smaller viscosity uncertainties. For instance, when considering ranges of electrical resistivity from the 2-D resistivity model for P2 in NW Fennoscandia (yellow patch, Fig. 6b), an increase in the ranges of water content (Fig. 6d), as well as in the ranges of viscosity (Fig. 6e), is evident compared to the cratonic domain (blue patch). Although the associated viscosity uncertainties for the cratonic domain are smaller than those for P2, this does not necessarily indicate that the viscosity model for the cratonic domain is more accurate and precise. Thus, care must be taken when interpreting the calculated viscosity uncertainty.

Many of the uncertainties in these geophysical inputs are not well constrained because uncertainty estimation from geophysical inversion is a challenging task. Most seismic and MT models are not published with calculated uncertainties, and experimental uncertainties often only reflect some of the experimental unknowns (e.g., Gardés et al., 2014). Therefore, the uncertainties we present here are an estimate based on current data and model assumptions for conversion. We hope that as data improve over time the uncertainties that can be calculated with our method will become both better constrained and smaller. In particular, probabilistic Bayesian geophysical inversions that produce quantified uncertainties in seismic wavespeed and electrical resistivity in each

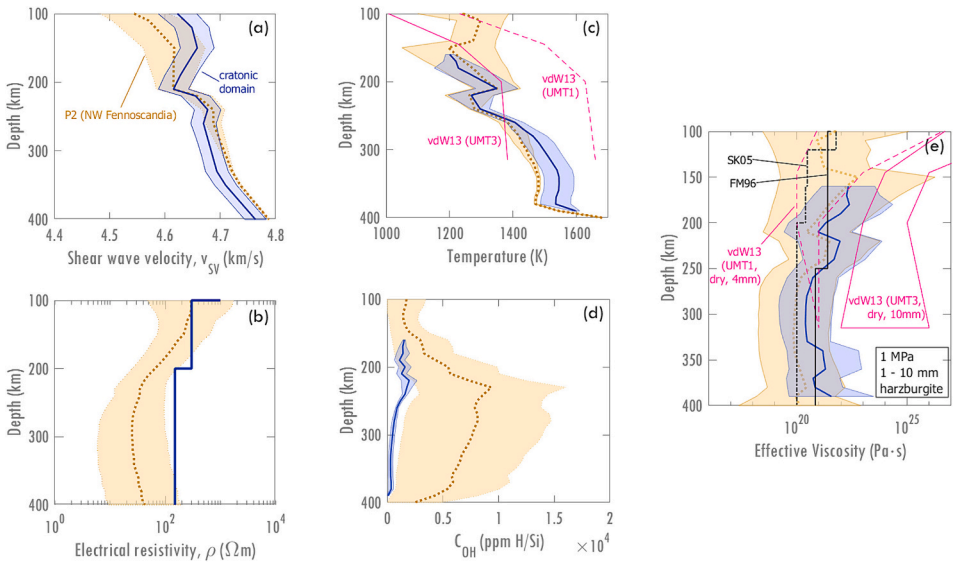

Fig. 6. Mantle structure of the cratonic domain versus NW Fennoscandia, particularly below P2. Shear wave velocities (a) and electrical resistivities (b) are averaged for the cratonic domain and P2 (areas indicated in Fig. 2a). The shear wave velocities and resistivities for the cratonic domain (blue lines) are as shown in Figs. 2b and 2c. While, the velocity and resistivity depth sections for P2 represent the extracted ranges of minimum and maximum values for each depth from 2-D profiles in Figs. 2e and 2h, respectively. Combining both (a) and (b) results in temperature (c), water content (d) and viscosity (e) models. The constructed viscosities are calculated for 1–10 mm grain sizes and 1 MPa stress. The FM96 (Forte and Mitrovica, 1996) and SK05 (Steffen and Kaufmann, 2005) viscosity profiles are GIA-constrained. The vdW13 (van der Wal et al., 2013; pink lines) thermal profiles (UMT1 and UMT3, which are derived from surface heat flow and seismic tomography, respectively) in (c) result in associated viscosity models in (e) for dry conditions and different grain sizes. (For interpretation of the references to colour in this figure legend, the reader is referred to the web version of this article.)

model cell (e.g., Manassero et al., 2021) will result in more accurate viscosity uncertainty estimation.

4.4.2. Model uncertainties

For the 1–10 mm grain sizes that we used in the viscosity calculation, diffusion and dislocation creep mechanisms co-exist (Fig. 7) producing larger viscosity uncertainty than for either diffusion creep or dislocation creep alone. Variations in water conditions also significantly affect the viscosity uncertainty. In particular, if the mantle at a given depth is inferred to be completely wet, its viscosity uncertainty is smaller than if it were dry or damp (e.g., the cratonic domain in Fig. 6d). This is attributed to the different values for laboratory-derived parameters (A, E^*, V^*, r) for different deformation mechanisms at dry and wet conditions. Since any assumption about composition affects the viscosity estimates through temperature and water content estimates, independent constraints on composition can improve viscosity models using our method.

The model parameter uncertainties (e.g., composition, grain size, stress) are difficult to quantify and therefore translate into overall viscosity uncertainties of several orders of magnitude, and are large when

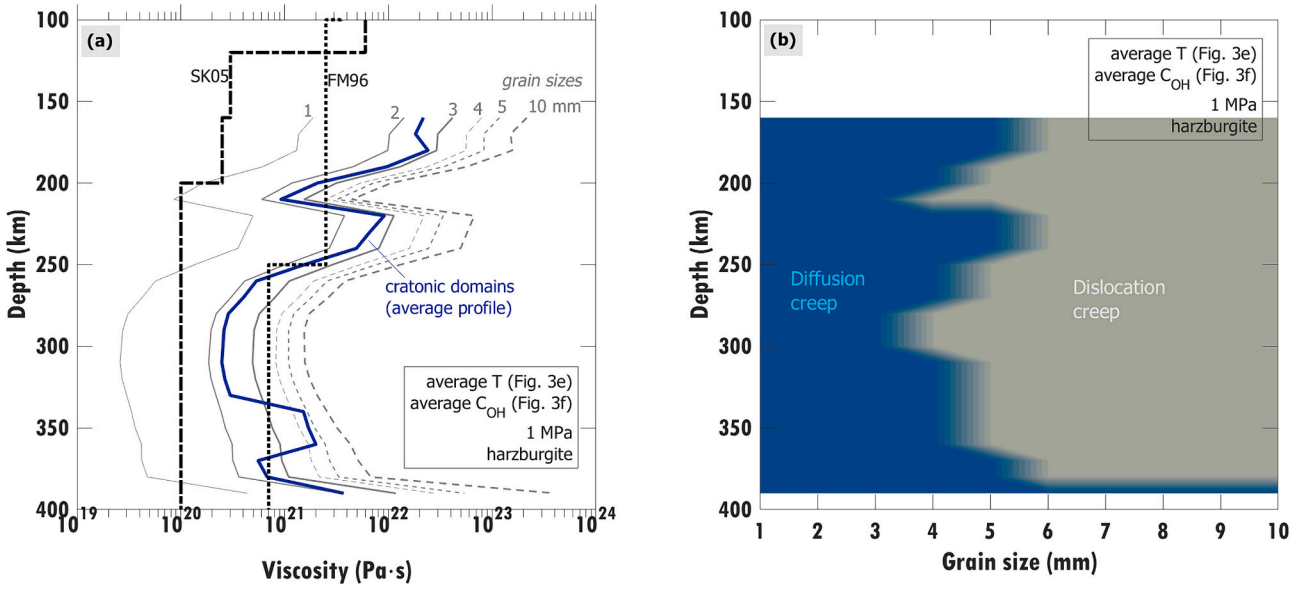

Fig. 7. Constructed viscosity structures (a) and dominant deformation mechanisms (b) for the Fennoscandian craton assuming harzburgite and a set of different olivine grain sizes (1–10 mm). The viscosity structures (grey lines in a) for different grain sizes are calculated using the inferred average temperatures (from Fig. 3e), average water contents (from Fig. 3f) and 1 MPa stress. The GIA viscosities SK05 and FM96 are shown in (a) for comparison.

compared to some GIA-constrained uncertainties, like those in Fennoscandia (e.g., Forte and Mitrovica, 1996; Milne et al., 2001; Steffen and Kaufmann, 2005) or upper mantle global averages (e.g., Lau et al., 2016). The strength of the method we propose here is that it can be used in places like the interiors of Greenland and Antarctica, where there are no GIA constraints, where global average models are insufficient to capture laterally varying viscosities (e.g., Milne et al., 2018), and where GIA must be constrained in order to produce more accurate calculations of ice sheet mass loss.

5. Geophysically-constrained viscosities versus GIA-constrained viscosities

In our calculation, the GIA-constrained viscosities are either on the low end or high end of the range of geophysically-constrained viscosities, which may be attributed to the olivine-only flow laws and the vertically polarized shear wave seismic model utilized in the viscosity calculation. Given that geophysically-derived viscosity estimates have historically been produced mostly from seismic data alone, and often without considering the impact of composition (e.g., Goes et al., 2000; Heeszel et al., 2016; Lucas et al., 2020), here we discuss in detail the impact of MT and composition for estimating viscosity using geophysical constraints.

5.1. Importance of MT constraints

Overall, when constraining lateral and radial viscosities for Fennoscandia, MT data are necessary to distinguish whether the upper mantle is wet or dry. MT data can also help to assess the plausible upper mantle composition (Section 5.2). We find here that MT constraints help to improve the geophysically-constrained viscosities such that they better agree with the GIA-constrained viscosities.

The 3-D viscosities of van der Wal et al. (2013) for Fennoscandia (pink polygons, Fig. 6e) are constrained by temperatures inferred from either surface heat flow (UMT1 thermal model, pink dashed line Fig. 6c) or seismic tomography (UMT3 thermal model, pink solid line) data. The authors have assumed either dry (0 ppm H/Si) or wet (1000 ppm H/Si) conditions for 4 mm or 10 mm grain size. For comparison, we have presented here their viscosity models for a dry olivine lithosphere with hot geotherm and 4-mm grain sizes (pink dashed polygon, Fig. 6e), and dry olivine lithosphere with a cold geotherm and 10-mm grain sizes (pink solid polygon). Of these, the dry and hotter lithosphere encompasses the GIA viscosities (black lines), while viscosities for the dry and colder lithosphere are much larger. If the actual temperature of the lithosphere is closer to UMT3, the lithosphere may require wet conditions to match the GIA viscosity constraints, which are consistent with our results (Fig. 6e).

Below 250 km, the northwestern Fennoscandian upper mantle, for instance beneath P2, is identified to be less viscous than the cratonic domain (Fig. 6). This decreased viscosity is not because of temperature – higher seismic velocity beneath northwestern Fennoscandia (Fig. 6a) indicates that the upper mantle there is actually colder than beneath the craton (Fig. 6c). Instead, it is because of greater water content (Fig. 6d), which is constrained by the resistivity profile (Fig. 6b). This additional hydration for northwestern Fennoscandia decreases average upper mantle viscosities such that they coincide with SK05 model (10^{20} Pa·s). We note that this result would not be possible without MT constraints, because seismic wave velocity cannot constrain water content.

5.2. Importance of composition

As suggested by Ramirez et al. (2022), composition should also be considered when estimating viscosity because composition affects both the seismic velocity and electrical resistivity and controls the amount of water that the upper mantle can hold. As constrained by seismic and MT, a wetter and colder harzburgite has viscosities that overlap with those of less wet (or even 'dry', defined as <100 ppm H/Si) and hotter pyrolite (Fig. 3g). This overlap is due to the tradeoff between temperature and water content for both viscosity and conductivity. As was mentioned before, this implies that knowledge of the composition will increase certainty about the viscosity.

The viscosity models of van der Wal et al. (2013) assume pure olivine, which translates to colder temperatures and higher viscosities than harzburgite (as seen in Fig. 3). Although the UMT3 geotherm coincides well with our thermal models for harzburgite (Fig. 6c), caution must be taken when interpreting both results. The UMT3 model is hotter than our thermal model for olivine (Fig. 3a), which may be attributed to a relatively high background temperature (average continental and oceanic geotherms for the upper mantle) that is used by van der Wal et al. (2013).

5.3. Inferred grain sizes and deformation mechanism

Applying the inferred average temperatures (blue line, Fig. 3e) and water content (blue line, Fig. 3f) for harzburgite, we calculate the viscosity structures for different grain sizes (grey lines, Fig. 7a) and the associated dominant deformation mechanism (Fig. 7b). We find that GIA-inferred viscosities for Fennoscandian upper mantle (below 250 km) would correspond to olivine grain sizes of 1–4 mm, and that the mantle would be deforming under diffusion creep. At the bottom of the lithosphere (between 150 and 250 km), that is interpreted via MT as wet (Fig. 3f), GIA-derived viscosities require <3 mm grain sizes. These small grain sizes may suggest that the inferred Fennoscandian lithosphere has high seismic attenuation, resulting in low seismic velocities (e.g., Ramirez et al., 2023). However, the significant amount of water within these depths may promote grain growth, particularly for those grains that deform via diffusion creep. Assuming that those inferred small grain sizes exist in the lithosphere, there must be other factors that suppress grain growth, i.e., pinning by other minerals, phase mixing, large ambient stresses, or low actual temperatures.

Another plausible argument is that the GIA-derived viscosities for the upper 250 km may be too small, either due to the assumed elastic lithosphere thickness or due to the insensitivity of the GIA data to shallow depths, particularly for melting of a broad ice sheet. The FM96 mantle viscosity model assumes an 80-km elastic lithosphere and uses joint inversion of long wavelength mantle convection and two geologically- and spatially-limited RSL datasets, which may result in a poorly resolved 1-D viscosity model for the upper 250 km. On the other hand, the SK05 mantle viscosity model assumes a 120-km lithosphere and utilizes good spatial RSL data, which yields lower viscosity estimates than FM96. The discrepancy between the two models is affected by the different elastic lithospheric thicknesses and the quality of RSL data.

5.4. Inferred lithosphere-asthenosphere boundary and low-viscosity zone

Petrologically, the lithosphere for cratonic Fennoscandia is interpreted to be 160–250 km thick (e.g., Kukkonen and Peltonen, 1999; Lehtonen et al., 2004). This is thicker than indicated by most GIA models (e.g., Forte and Mitrovica, 1996; Steffen and Kaufmann, 2005; Root et al., 2015), but agrees with MT constraints (Fig. 2c), regional P-wave tomography (Bulut et al., 2022) and mantle heat flow models (Veikkolainen et al., 2017). Because our viscosity models are based on such geophysical constraints, we infer a significant decrease in viscosity for the cratonic domain (by 1–2 orders of magnitude) at approximately 240 km, which may represent the lithosphere-asthenosphere boundary (Fig. 6e). Below this thick lithosphere, a low-viscosity asthenosphere may exist at larger depths beneath the craton (e.g., Gung et al., 2003; Cathles et al., 2023). Our results suggest a cratonic asthenosphere that is ~100 km thick with an average viscosity of about 2.5×10^{20} Pa·s (Fig. 6e). For comparison, Fjeldskaar (1994, 1997) proposed that the Fennoscandian asthenosphere must be <100 km thick with a viscosity < 7×10^{19} Pa·s, although an even thinner (75 km or less) and weaker

($\sim 10^{19}$ Pa·s) asthenosphere would also be consistent with the transgression history of Fennoscandia (Fjeldskaar and Amantov, 2018). Although the thick lithosphere and low-viscosity asthenosphere suggested here are not evident in the GIA-constrained viscosity profiles, this could be due to the poor resolving power of GIA data for the shallow Earth. Our geophysically-constrained calculation shows that a potential low-viscosity asthenosphere is present below 250 km, with a minimum viscosity of $\sim 10^{19.2}$ Pa·s for the cratonic domain and $\sim 10^{18.1}$ Pa·s for northwestern Fennoscandia (Fig. 6e). The low-viscosity zone beneath northwestern Fennoscandia is less viscous than for the cratonic domain because of its extra water. Such variation in water contents stems from the different resistivity profiles between northwestern Fennoscandia and the cratonic domain (Fig. 6b), which are affected by the different tectonic units involved (i.e., Proterozoic and Archean lithospheres; Cherevatova et al., 2015).

Although the lithosphere for the cratonic domain (above 250 km) is wetter than the asthenosphere below it, the lithosphere is still more viscous than the asthenosphere due to its lower temperatures. Within the asthenosphere, the viscosity decreases in response to an increasing temperature. However, water content variations can produce significant viscosity variations, particularly if transitioning from wet to dry (or vice versa) conditions. This occurs in the cratonic domain between 330 km and 360 km depth (Fig. 6e), where possible dry conditions (Fig. 6d) induce high viscosities with deformation occurring under the DisGBS mechanism.

This study infers a wetter lithosphere (~1000–2000 ppm H/Si, Fig. 6d) above 250 km and a less wet mantle (<1000 ppm H/Si, including the suggested asthenosphere) below 250 km for the cratonic domain (Fig. 6d) compared to what Hirth et al. (2000) suggested for the Superior Craton, which Hirth et al. (2000) proposed to be a dry Archean craton with underlying wet (>1000 ppm H/Si) mantle. This discrepancy can be attributed to differences in electrical conductivities beneath the different cratons, and different choices for thermal profiles and bulk compositions between the studies. Our seismically-determined thermal profiles are colder than those used by Hirth et al. (2000), who constrained geotherms from xenoliths and surface heat flow data for the Superior Province. If the Fennoscandian lithosphere is indeed colder than that of the Superior Province, it must be wet in order to explain its higher conductivity. As for the asthenosphere, the less conductive and colder Fennoscandian asthenosphere is expected to have less water than the more conductive and hotter asthenosphere below the Superior Province. In both regions, the sensitivities of the MT models are likely to be decreasing at asthenospheric depths, and probabilistic MT models would quantify the possible ranges of asthenospheric resistivities more accurately.

Our analysis of regional seismic data for the Norway-Sweden and Finland regions suggests that both regions have wet lower lithosphere (between 150 km depth and the deeper lithosphere-asthenosphere boundary) despite different thermal profiles, consistent with the overall cratonic domain (Fig. 4). With the assumption that the 1-D MT data available for Fennoscandia reflect the mantle beneath both regions, we infer lateral and radial water heterogeneities across Fennoscandia, which are necessary to explain temperature variations determined using seismic constraints. Results suggest that water content increases from Norway-Sweden to Finland and generally decreases with depth (Fig. 8). Such heterogeneity imposes difficulties in fitting sea level and uplift rate data simultaneously (van der Wal et al., 2013). We interpret the presence of low-viscosity asthenosphere across Fennoscandia from seismic and MT constraints. This asthenosphere is deeper than suggested by Fjeldskaar (1994, 1997) and has a varying thickness and depth (Fig. 8). In particular, a thin and shallow low-viscosity asthenospheric zone is present beneath Norway-Sweden and becomes thicker and deeper towards Finland. Interestingly, the low-viscosity layer present between 200 and 240 km depth beneath Norway-Sweden (Fig. 4c) is 40 km deeper than the low-viscosity layer inferred for (mainly) Sweden-Finland from a viscosity inversion constrained by localized crustal uplift data (from the BIFROST project; Fig. 6b in Steffen and Kaufmann, 2005). We expect that such lateral and radial variations of the low-viscosity asthenosphere, if present, reflect complexities in predicting GIA responses to deglaciation in the vicinity of large lateral variations in viscosity (e.g., Weerdesteijn et al., 2022).

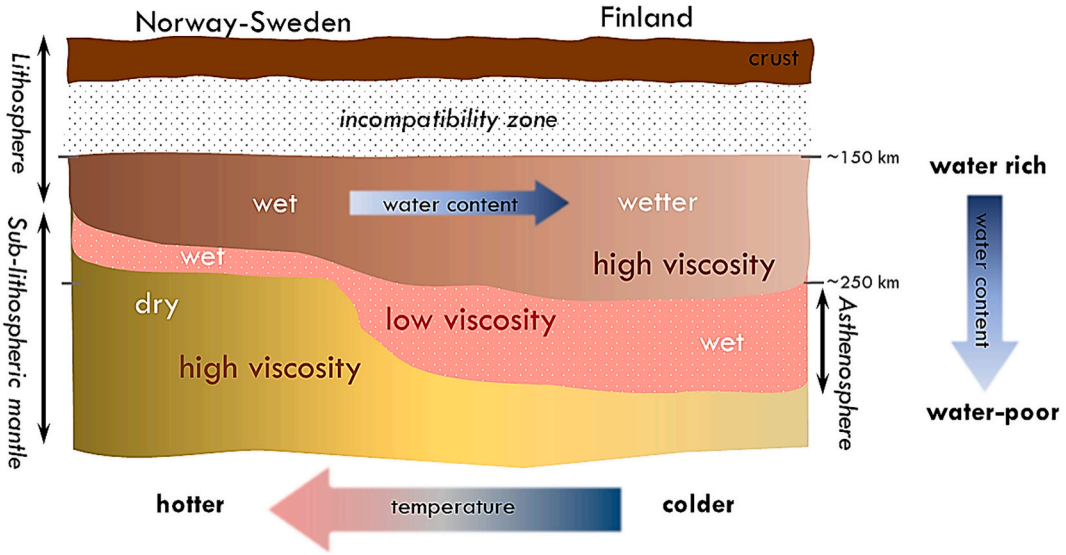

Fig. 8. A schematic diagram of the lithosphere and sub-lithospheric mantle structures beneath Fennoscandia in terms of their water content, temperature, and viscosity, as inferred from regional seismic and MT data jointly analyzed across Fennoscandia. Incompatibility between seismic and MT constraints complicate interpretations shallower than 150 km depth (see text). Looking deeper, we infer a lithosphere-asthenosphere boundary that deepens moving eastward from Norway-Sweden (left) to Finland (right), and lithospheric thicknesses that vary from 200 to 250 km (thicker than inferred from most GIA models). The lower lithosphere becomes wetter and colder moving eastward, which suggests a lateral variation in lithospheric viscosity. The underlying low-viscosity asthenosphere also deepens and thickens moving eastward, following variations in temperature and water content. The seismic and MT data also suggest decreasing water content with depth, implying larger viscosities beneath the asthenosphere. The seismic and MT constraints thus image the viscosity structure beneath Fennoscandia, which varies both laterally and with depth.

6. Conclusions

Seismic anomalies may be attributed to thermal variations that translate into viscosity variations. However, compositional heterogeneities may also contribute to the observed seismic velocity variations. By integrating MT constraints into our analysis and assuming pure olivine, harzburgite and pyrolite compositions, we conclude that (i) our geophysically-constrained viscosities are better resolved because of better constraints on water content, and (ii) Fennoscandian upper mantle below 250 km is likely to be a wet harzburgite with lateral and radial viscosity magnitudes ranging within $10^{19.2} - 10^{23.5}$ Pa·s when assuming 1–10 mm grain sizes and 1 MPa stress. A hotter and dry pyrolytic upper mantle may alternatively exist with slightly higher viscosities compared to a colder and wet harzburgite. This highlights that potential compositional variations introduce a tradeoff between water content and temperature when estimating viscosities. Xenolith data, which can improve composition constraints, can thus improve geophysically-constrained viscosity estimates, particularly in the lithospheric mantle where a fertile composition with conductive phases may be present (Özaydin et al., 2021; Selway, 2014). A pure olivine assumption results in significantly higher viscosity estimates that do not agree with the GIA-derived viscosities.

Lateral and radial variations in viscosity are likely across Fennoscandia due to heterogeneities in temperature and water content (Fig. 8), and potentially also composition. To constrain such viscosity variations, including along northern and western coastal areas of Fennoscandia where viscosities may be low, regional MT and seismic tomography models with good upper mantle resolution are required. Such high-resolution data can provide additional constraints on a potential low-viscosity zone, which may be present below 250 km depth across Fennoscandia.

The viscosities constrained from seismic and MT observations using the method of Ramirez et al. (2022) broadly agree with the viscosities for Fennoscandia, as constrained from GIA. This suggests that this method can be applied in regions where GIA-constrained upper mantle viscosities are not available, as is the case for most regions of the world, including polar regions where improved GIA models would lead to more accurate estimates of present-day ice mass loss. Furthermore, the method can detect lateral variations in mantle viscosity because seismic and MT data are sensitive to lateral variations in mantle parameters (water and temperature) that relate to viscosity. Incorporating lateral viscosity variations into GIA modeling is of great importance because such variations may greatly affect GIA uplift rate predictions. In particular, low-viscosity regions of the sub-lithospheric mantle may facilitate rapid GIA uplift (e.g., Weerdesteijn et al., 2022). Here we identify the northwestern coast of Fennoscandia as one such low-viscosity region. With the assumption that the 1-D MT model for Fennoscandia also reflects the subsurface of Norway-Sweden, we identify the presence of thin and shallow low-viscosity asthenosphere that becomes thicker and deeper towards Finland (Fig. 8). Thus, data from regional magnetotelluric surveys, when combined with regional seismic data, can help to accurately identify such low-viscosity regions.

Credit author statement

Florence D.C. Ramirez: Conceptualization, Formal analysis, Investigation, Methodology, Visualization, Writing – original draft.

Kate Selway: Conceptualization, Formal analysis, Supervision, Writing – Review & Editing, Funding Acquisition.

Clinton P. Conrad: Conceptualization, Formal analysis, Supervision, Writing – Review & Editing, Funding Acquisition.

Valerie Maupin: Writing – Review & Editing; Data Curation.

Maxim Smirnov: Writing – Review & Editing, Data Curation.

Composition and structure of the mantle; Europe; Magnetotellurics and Seismic tomography; Joint inversion; Cratons; Rheology: mantle.

CRediT authorship contribution statement

Florence D.C. Ramirez: Formal analysis, Investigation, Methodology, Visualization, Writing – original draft. **Kate Selway:** Funding acquisition, Supervision, Writing – review & editing, Conceptualization. **Clinton P. Conrad:** Conceptualization, Funding acquisition, Supervision, Writing – review & editing. **Valerie Maupin:** Data curation, Writing – review & editing. **Maxim Smirnov:** Data curation, Writing – review & editing.

Declaration of competing interest

The authors declare that they have no known competing financial interests or personal relationships that could have appeared to influence the work reported in this paper.

Data availability

No data was used for the research described in the article.

Acknowledgments

This work was partly supported by the Research Council of Norway via project 288449 (MAGPIE project) and via its Centres of Excellence scheme, project numbers 223272 (CEED) and 332523 (PHAB), and partly by the Australian Research Council grant FT1500100541. We thank Andrea Tommasi, Rhodri Davies and two anonymous reviewers for valuable inputs that significantly improved this manuscript. We also thank the editor, Ana Ferreira, for handling the manuscript.

References

Austermann, J., Hoggard, M., Latychev, K., Richards, F., Mitrovica, J.X., 2021. The effect of lateral variations in Earth structure on Last Interglacial sea level. Geophys. J. Int. 227 (3), 1938–1960. https://doi.org/10.1093/gji/ggab289.

Babuska, V., Cara, M., 1991. Seismic Anisotropy in the Earth. Kluwer Academic Publishers, The Netherlands.

Ball, P.W., White, N.J., Maclennan, J., Stephenson, S.N., 2021. Global influence of mantle temperature and plate thickness on intraplate volcanism. Nat. Commun. 12 (1), 2045. https://doi.org/10.1038/s41467-021-22323-9.

Baptiste, V., Tommasi, A., Demouchy, S., 2012. Deformation and hydration of the lithospheric mantle beneath the Kaapvaal craton, *South Africa*. Lithos 149, 31–50. https://doi.org/10.1016/j.lithos.2012.05.001.

Barnhoorn, A., van der Wal, W., Vermeersen, B., Drury, M., 2011. Lateral, radial, and temporal variation in upper mantle viscosity and rheology under Scandinavia. Geochem. Geophys. Geosyst. 12, 1–19. https://doi.org/10.1029/2010GC003290.

Bercovici, D., Skemer, P., 2017. Grain damage, phase mixing and plate-boundary formation. J. Geodyn. 108, 40–55. https://doi.org/10.1016/j.jog.2017.05.002.

Beyer, E., Griffin, W., O'Reily, S., 2006. Transformation of Archaean lithospheric mantle by refertilization: evidence from exposed peridotites in the Western Gneiss Region, Norway. J. Petrol. 47, 1611–1636. https://doi.org/10.1093/petrology/egl022.

Bogdanova, S.V., Pashkevich, I.K., Gorbatschev, R., Orlyuk, M.I., 1996. Riphean rifting and major Palaeoproterozoic crustal boundaries in the basement of the East European Craton: geology and geophysics. Tectonophysics 268, 1–21. https://doi.org/10.1016/S0040-1951(96)00232-6.

Bruneton, M., Pedersen, H., Vacher, P., Kukkonen, I., Arndt, N., Funke, S., Friederich, W., Farra, V., SVEKALAPKO Seismic Tomography Working Group, 2004. Layered lithospheric mantle in the Central Baltic shield from surface waves and xenolith analysis. Earth Planet. Sci. Lett. 226, 41–52. https://doi.org/10.1016/j.epsl.2004.07.034.

Bulut, N., Thybo, H., Maupin, V., 2022. Highly heterogeneous upper-mantle structure in Fennoscandia from finite-frequency P-body-wave tomography. https://doi.org/10.1093/gji/ggac107.

Calcagnile, G., 1982. The lithosphere-asthenosphere system in Fennoscandia. Tectonophysics 90, 19–35. https://doi.org/10.1016/0040-1951(82)90251-7.

Cathles, L., Fjeldskar, W., Lenardic, A., Romanowicz, B., Seales, J., Richards, M., 2023. Influence of the asthenosphere on earth dynamics and evolution. Sci. Rep. 13 (1), 13367. https://doi.org/10.1038/s41598-023-39973-y.

Chen, S., Hiraga, T., Kohlstedt, D.L., 2006. Water weakening of clinopyroxene in the dislocation creep regime. J. Geophys. Res. 111 (B8), B08203. https://doi.org/10.1029/2005JB003885.

Cherevatova, M., Smirnov, M. Yu, Jones, A.G., Pedersen, L.B., MaSca Working Group, Becken, M., Biolik, M., Cherevatova, M., Ebbing, E., Gradmann, S., Gurk, M., Hübert, J., Jones, A.G., Junge, A., Kamm, J., Korja, T., Lahti, I., Löwer, A., Nittinger, C., Pedersen, L.B., Savvaidis, A., Smirnov, M., 2015. Magnetotelluric array

data analysis from north-west Fennoscandia. Tectonophysics 653, 1–19. https://doi.org/10.1016/j.tecto.2014.12.023.
Cordellier, F., Boudier, F., Boullier, A.M., 1981. Structural study of the Almklovdalen peridotite massif (southern Norway). Tectonophysics 77, 257–281. https://doi.org/10.1016/0040-1951(81)90266-3.
Creel, R.C., Austermann, J., Khan, N., D'Andrea, W., Balascio, N., Dyer, B., Ashe, E., Menke, W., 2022. Postglacial relative sea level change in Norway. Quat. Sci. Rev. 282, 107422 https://doi.org/10.1016/j.quascirev.2022.107422.
Davies, D.R., Valentine, A.P., Kramer, S.C., Rawlinson, N., Hoggard, M.J., Eakin, C.M., Wilson, C.R., 2019. Earth's multi-scale topographic response to global mantle flow. Nat. Geosci. 12 (10), 845–850. https://doi.org/10.1038/s41561-019-0441-4.
Dixon, J., Dixon, T.H., Bell, D.R., Malservisi, R., 2004. Lateral variation in upper mantle viscosity: role of water. Earth Planet. Sci. Lett. 222, 451–467. https://doi.org/10.1016/j.epsl.2004.03.022.
Eken, T., Shomali, Z.H., Roberts, R., Hieronymus, C.F., Bodvarsson, R., 2008. S and P velocity heterogeneities within the upper mantle below the Baltic Shield. Tectonophysics 462 (1–4), 109–124. https://doi.org/10.1016/j.tecto.2008.02.015.
Fjeldskaar, W., 1994. Viscosity and thickness of the asthenosphere detected from the Fennoscandian uplift. Earth Planet. Sci. Lett. 126 (4), 399–410. https://doi.org/10.1016/0012-821X(94)90120-1.
Fjeldskaar, W., 1997. Flexural rigidity of Fennoscandia inferred from the postglacial uplift. Tectonics 16, 596–608. https://doi.org/10.1029/97TC00813.
Fjeldskaar, W., Amantov, A., 2018. Younger Dryas transgression in western Norway: a modelling approach. Nor. J. Geol. 98 (1), 127–139. https://doi.org/10.17850/njg98-1-08.
Forte, A.M., Mitrovica, J.X., 1996. New inferences of mantle viscosity from joint inversion of long-wavelength mantle convection and post-glacial rebound data. Geophys. Res. Lett. 23, 1147–1150. https://doi.org/10.1029/96GL00964.
Gardés, E., Gaillard, F., Tarits, P., 2014. Toward a unified hydrous olivine electrical conductivity law. Geochem. Geophys. Geosyst. 15 (12), 4984–5000. https://doi.org/10.1002/2014GC005496.
Goes, S., Govers, R., Vacher, P., 2000. Shallow mantle temperatures under Europe from P and S wave tomography. J. Geophys. Res. 105 (B5), 11153–11169. https://doi.org/10.1029/1999jb900300.
Gung, Y., Panning, M., Romanowicz, B., 2003. Global anisotropy and the thickness of continents. Nature 422, 707. https://doi.org/10.1038/nature01559.
Hansen, L., Warren, J., 2015. Quantifying the effect of pyroxene on deformation of peridotite in a natural shear zone. J. Geophys. Res. Solid Earth 120 (4), 2717–2738. https://doi.org/10.1002/2014JB011584.
Haskell, N., 1935. The motion of a viscous fluid under a surface load. Physics 6, 265. https://doi.org/10.1063/1.1745329.
Hasterok, D., Chapman, D.S., 2011. Heat production and geotherms for the continental lithosphere. Earth Planet. Sci. Lett. 307, 59–70. https://doi.org/10.1016/j.epsl.2011.04.034.
Heeszel, D., Wiens, D.W., Anandakrishnan, S., Aster, R., Dalziel, I., Huerta, A., et al., 2016. Upper mantle structure of central and West Antarctica from array analysis of Rayleigh wave phase velocities. J. Geophys. Res. Solid Earth 121 (3), 1758–1775. https://doi.org/10.1002/2015JB012616.
Hill, E., Davis, J., Tamisiea, M., Lindberg, M., 2010. Combination of geodetic observations and models for glacial isostatic adjustment fields in Fennoscandia. J. Geophys. Res. 115, B07403. https://doi.org/10.1029/2009JB006967.
Hirth, G., Kohlstedt, D., 2003. Rheology of the upper mantle and the mantle wedge: a view from the experimentalists. Inside the Subduction Factory. Geophys. Monogr. 138, 83–105. https://doi.org/10.1029/138GM0 6.
Hirth, G., Evans, R., Chave, A., 2000. Comparison of continental and oceanic mantle electrical conductivity: is the Archean lithosphere dry? Geochem. Geophys. Geosyst. 1 (12) https://doi.org/10.1029/2000GC000048.
Johansson, J., Davis, J., Scherneck, H.-G., Milne, G., Vermeer, M., Mitrovica, J., Bennett, R., Jonsson, B., Elgered, G., Elosegui, P., Koivula, H., Poutanen, M., Rönnäng, B., Shapiro, I., 2002. Continuous GPS measurements of postglacial adjustment in Fennoscandia 1. Geodetic results. J. Geophys. Res. 107, B82157. https://doi.org/10.1029/2001JB000400.
Kaufmann, G., Wu, P., 2002a. Glacial isostatic adjustment on a three-dimensional laterally heterogeneous earth: examples from Fennoscandia and the Barents Sea. Ice Sheets, Sea Level and the Dynamic Earth Geodynamics Series 29. https://doi.org/10.1002/9781118670101.ch18.
Kaufmann, G., Wu, P., 2002b. Glacial isostatic adjustment in Fennoscandia with a three-dimensional viscosity structure as an inverse problem. Earth Planet. Sci. Lett. 197, 1–10. https://doi.org/10.1016/S0012-821X(02)00477-6.
Kennett, B.L.N., Engdahl, E.R., Buland, R., 1995. Constraints on seismic velocities in the Earth from traveltimes. Geophys. J. Int. 122 (1), 108–124. https://doi.org/10.1111/j.1365-246X.1995.tb03540.x.
Kierulf, H.P., Steffen, H., Simpson, M.J., Lidberg, M., Wu, P., Wang, H., 2014. A GPS velocity field for Fennoscandia and a consistent comparison to glacial isostatic adjustment models. J. Geophys. Res. Solid Earth 119, 6613–6629. https://doi.org/10.1002/2013JB010889.
Kierulf, H.P., Steffen, H., Barletta, V., Lidberg, M., Johansson, J., Kristiansen, O., Tarasov, L., 2021. A GNSS velocity field for geophysical applications in Fennoscandia. J. Geodyn. 146, 101845 https://doi.org/10.1016/j.jog.2021.101845.
Klöcking, M., White, N.J., Maclennan, J., McKenzie, D., Fitton, J.G., 2018. Quantitative relationships between basalt geochemistry, shear wave velocity, and asthenospheric temperature beneath western north america. Geochem. Geophys. Geosyst. 19 (9), 3376–3404. https://doi.org/10.1029/2018GC007559.
Kukkonen, I.T., Peltonen, P., 1999. Xenolith-controlled geotherm for the central Fennoscandian Shield: implications for lithosphere-asthenosphere relations. Tectonophysics 304, 301–315. https://doi.org/10.1016/S0040-1951(99)00031-1.
Kukkonen, I.T., Kinnunen, K.A., Peltonen, P., 2003. Mantle xenoliths and thick lithosphere in the Fennoscandian Shield. Phys. Chem. Earth 28, 349–360. https://doi.org/10.1016/S1474-7065(03)00057-3.
Lambeck, K., Smither, C., Ekman, M., 1998a. Tests of glacial rebound models for Fennoscandia based on instrumented sea- and lake-level records. Geophys. J. Int. 135, 375–387. https://doi.org/10.1046/j.1365-246X.1998.00643.x.
Lambeck, K., Smither, C., Johnston, P., 1998b. Sea-level change, glacial rebound and mantle viscosity for northern Europe. Geophys. J. Int. 134 (1), 102–144. https://doi.org/10.1046/j.1365-246x.1998.00541.x.
Lambeck, K., Purcell, A., Zhao, J., Svensson, N.-O., 2010. The Scandinavian ice Sheet: from MIS 4 to the end of the Last Glacial Maximum. Boreas 39, 410–435. https://doi.org/10.1111/j.1502-3885.2010.00140.x.
Lau, H.C.P., Mitrovica, J.X., Austermann, J., Crawford, O., Al-Attar, D., Latychev, K., 2016. Inferences of mantle viscosity based on ice age data sets: radial structure. JGR Solid Earth 121 (10), 6991–7012. https://doi.org/10.1002/2016JB013043.
Lebedev, S., Boonen, J., Trampert, J., 2009. Seismic structure of Precambrian lithosphere: new constraints from broad-band surface-wave dispersion. Lithos 109 (1–2), 96–111. https://doi.org/10.1016/j.lithos.2008.06.010.
Lehtonen, M.L., O'Brien, H.E., Peltonen, P., Johanson, B.S., Pakkanen, L.K., 2004. Layered mantle at the Karelian Craton margin: P – T of mantle xenocrysts and xenoliths from the Kaavi – Kuopio kimberlites, Finland. Lithos 77, 593–608. https://doi.org/10.1016/j.lithos.2004.04.026.
Lidberg, M., Johansson, J., Scherneck, H.-G., Davis, J., 2007. An improved and extended GPS-derived 3D velocity field of the glacial isostatic adjustment (GIA) in Fennoscandia. J. Geodyn. 81, 213–230. https://doi.org/10.1007/s00190-006-0102-4.
Lucas, E., Soto, D., Nyblade, A.A., Lloyd, A., Aster, R., Wiens, D., et al., 2020. P- and S-wave velocity structure of central West Antarctica: implications for the tectonic evolution of the West Antarctic rift system. Earth Planet. Sci. Lett. 546, 116437 https://doi.org/10.1016/j.epsl.2020.116437.
Manassero, M.C., Afonso, J.C., Zyserman, F.I., Jones, A.G., Zlotnik, S., Fomin, I., 2021. A reduced order approach for probabilistic inversions of 3D magnetotelluric data II: joint inversion of MT and surface-wave data. JGR Solid Earth 126 (12). https://doi.org/10.1029/2021JB021962 e2021JB021962.
Marotta, A.M., Mitrovica, J.X., Sabadini, R., Milne, G., 2004. Combined effects of tectonics and glacial isostatic adjustment on intraplate deformation in central and northern Europe: applications to geodetic baseline analyses. J. Geophys. Res. 109, B01413. https://doi.org/10.1029/2002JB002337.
Mauerberger, A., Sadeghisorkhani, H., Maupin, V., Gudmundsson, O., Tilmann, F., 2022. A shear-wave velocity model for the Scandinivian lithosphere from Rayleigh waves and ambient noise – implications for the origin of the topography of the Scandes mountain range. Tectonophysics 838, 229507. https://doi.org/10.1016/j.tecto.2022.229507.
Maupin, V., Mauerberger, A., Tilmann, F., 2022. The radial anisotropy of the continental lithosphere from analysis of love and Rayleigh wave phase velocities in Fennoscandia. JGR Solid Earth 127. https://doi.org/10.1029/2022JB024445 e2022JB024445.
Milne, G.A., Davis, J., Mitrovica, J.X., Scherneck, H.-G., Johansson, J., Vermeer, M., Koivula, H., 2001. Space-geodetic constraints on glacial isostatic adjustment in Fennoscandia. Science 291, 2381–2385. https://doi.org/10.1126/science.1057022.
Milne, G.A., Mitrovica, J.X., Scherneck, H.-G., Davis, J., Johansson, J., Koivula, H., Vermeer, M., 2004. Continuous GPS measurements of postglacial adjustment in Fennoscandia: 2. Modeling results. J. Geophys. Res. 109, B02412. https://doi.org/10.1029/2003JB002619.
Milne, G.A., Latychev, K., Schaeffer, A., Crowley, J.W., Lecavalier, B.S., Audette, A., 2018. The influence of lateral earth structure on glacial isostatic adjustment in Greenland. Geophys. J. Int. 214 (2), 1252–1266. https://doi.org/10.1093/gji/ggy189.
Mints, M., Glaznev, V., Muraniva, O., Sokolova, E.Y., 2020. 3D model of Svecofennian accretionary Orogen and Karelia Craton base don geology, reflection seismics, magnetotellurics and density modelling: geodynamic speculations. Geosci. Front. 11, 999–1023. https://doi.org/10.1016/j.gsf.2019.10.003.
O'Donnell, J., Selway, K., Nyblade, A., Brazier, R., Wiens, D., Anandakrishnan, S., et al., 2017. The uppermost mantle seismic velocity and viscosity structure of central West Antarctica. Earth Planet. Sci. Lett. 472, 38–49. https://doi.org/10.1016/j.epsl.2017.05.016.
Özaydin, S., Selway, K., 2020. MATE: an analysis tool for the interpretation of magnetotelluric models of the mantle. Geochem. Geophys. Geosyst. 21, 1–26. https://doi.org/10.1029/2020GC009126.
Özaydin, S., Selway, K., Griffin, W.L., 2021. Are xenoliths from southwestern Kaapvaal craton representative of the broader mantle? Constraints from magnetotelluric modeling. Geophys. Res. Lett. 48 https://doi.org/10.1029/2021GL092570 e2021GL092570.
Padrón-Navarta, J., Hermann, J., 2017. A subsolidus olivine water solubility equation for the Earth's Upper Mantle. J. Geophys. Res. Solid Earth 122, 9862–9880. https://doi.org/10.1002/2017JB014510.
Paulson, A., Zhong, S., Wahr, J., 2005. Modelling post-glacial rebound with lateral viscosity variations. Geophys. J. Int. 163, 357–371. https://doi.org/10.1111/j.1365-246X.2005.02645.x.
Pedersen, H., Bruneton, M., Maupin, V., SVEKALAPKO Seismic Tomography Working Group, 2006. Lithopsheric and sublithospheric anisotropy beneath the Baltic shield from surface-wave array analysis. Earth Planet. Sci. Lett. 244, 590–605. https://doi.org/10.1016/j.epsl.2006.02.009.
Ramirez, F.D.C., Selway, K., Conrad, C.P., Lithgow-Bertelloni, C., 2022. Constraining upper mantle viscosity using temperature and water content inferred from seismic

and magnetotelluric data. J. Geophys. Res. Solid Earth 127 (8), E2021JB023824. https://doi.org/10.1029/2021JB023824.
Ramirez, F.D.C., Conrad, C.P., Selway, K., 2023. Grain size reduction by plug flow in the wet oceanic upper mantle explains the asthenosphere's low seismic Q zone. Earth Planet. Sci. Lett. 616, 118232 https://doi.org/10.1016/j.epsl.2023.118232.
Romanowicz, B., 1995. A global tomographic model of shear attenuation in the upper mantle. J. Geophys. Res. 100 (B7), 12375–12394. https://doi.org/10.1029/95jb00957.
Root, B.C., van der Wal, W., Novák, P., Ebbing, J., Vermeersen, L.L.A., 2015. Glacial isostatic adjustment in the static gravity field of Fennoscandia. J. Geophys. Res. Solid Earth 120 (1), 503–518. https://doi.org/10.1002/2014JB011508.
Rosentau, A., Klemann, V., Bennike, O., Steffen, H., Wehr, J., et al., 2021. A Holocene relative sea-level database for the Baltic Sea. Quat. Sci. Rev. 266, 1070714. https://doi.org/10.1016/j.quascirev.2021.107071.
Schaeffer, A.J., Lebedev, S., 2013. Global shear speed structure of the upper mantle and transition zone. Geophys. J. Int. 194, 417–449. https://doi.org/10.1093/gji/ggt095.
Schotman, H., Vermeersen, L., Wu, P., Drury, M., de Bresser, J., 2009. Constraints on shallow low-viscosity zones in northern Europe from future GOCE gravity data. Geophys. J. Int. 178, 65–84. https://doi.org/10.1111/j.1365-246X.2009.04160.x.
Selway, K., 2014. On the causes of electrical conductivity anomalies in tectonically stable lithosphere. Surv. Geophys. 35, 219–257. https://doi.org/10.1007/s10712-013-9235-1.
Selway, K., 2018. Electrical discontinuities in the continental lithosphere imaged with magnetotellurics. In: Geophysical Monograph Series, Chapter 5. https://doi.org/10.1002/9781119249740.ch5.
Selway, K., Yi, J., Karato, S.-I., 2014. Water content of the Tanzanian lithosphere from magnetotelluric data: implications for cratonic growth and stability. Earth Planet. Sci. Lett. 388, 175–186. https://doi.org/10.1016/j.epsl.2013.11.024.
Selway, K., O'Donnell, J.P., Özaydin, S., 2019. Upper mantle melt distribution from petrologically constrained magnetotellurics. Geochem. Geophys. Geosyst. 20 (7), 3328–3346. https://doi.org/10.1029/2019GC008227.
Steffen, H., Kaufmann, G., 2005. Glacial isostatic adjustment of Scandinivia and northwestern Europe and the radial viscosity structure of the Earth's mantle. Geophys. J. Int. 163, 801–812. https://doi.org/10.1111/j.1365-246X.2005.02740.x.
Steffen, H., Wu, P., 2011. Glacial isostatic adjustment in Fennoscandia – a review of data and modeling. J. Geodyn. 52, 169–204. https://doi.org/10.1016/j.jog.2011.03.002.
Steffen, H., Kaufmann, G., Wu, P., 2006. Three-dimensional finite-element modeling of the glacial isostatic adjustment in Fennoscandia. Earth Planet. Sci. Lett. 250, 358–375. https://doi.org/10.1016/j.epsl.2006.08.003.
Steffen, H., Wu, P., Wang, H., 2010. Determination of the Earth's structure in Fennoscandia from GRACE and implications for the optimal post-processing of GRACE data. Geophys. J. Int. 182, 1295–1310. https://doi.org/10.1111/j.1365-246X.2010.04718.x.
Stixrude, L., Lithgow-Bertelloni, C., 2005. Thermodynamics of mantle minerals - I. Physical properties. Geophys. J. Int. 162, 610–632. https://doi.org/10.1111/j.1365-246X.2005.02642.x.
Stixrude, L., Lithgow-Bertelloni, C., 2011. Thermodynamics of mantle minerals - II. Phase equilibria. Geophys. J. Int. 184, 1180–1213. https://doi.org/10.1111/j.1365-246X.2010.04890.x.
Stroeven, A.P., et al., 2016. Deglaciation of Fennoscandia. Quat. Sci. Rev. 147, 91–121. https://doi.org/10.1016/j.quascirev.2015.09.016.
Tasaka, M., Zimmerman, M.E., Kohlstedt, D.L., 2020. Rheological weakening of olivine + orthopyroxene aggregates due to phase mixing: effects of orthopyroxene volume fraction. J. Geophys. Res. Solid Earth 125 (9), e2020JB019888. https://doi.org/10.1029/2020JB019888.
Torsvik, T.H., Burke, K., Steinberger, B., Webb, S.J., Ashwal, L.D., 2010. Diamonds sampled by plumes from the core-mantle boundary. Nature 466 (7304), 352–355. https://doi.org/10.1038/nature09216.
van der Wal, W., Ijpelaar, T., 2017. The effect of sediment loading in Fennoscandia and the Barents Sea during the last glacial cycle on glacial isostatic adjustment observations. Solid Earth 8 (5), 955–968. https://doi.org/10.5194/se-8-955-2017.
van der Wal, W., Barnhoorn, A., Stocchi, P., Gradmann, S., Wu, P., Drury, M., Vermeersen, B., 2013. Glacial isostatic adjustment model with composite 3-D Earth rheology for Fennoscandia. Geophys. J. Int. 194, 61–77. https://doi.org/10.1093/gji/ggt099.
Varentsov, I.M., Engels, M., Korja, T., Smirnov, M., the BEAR Working Group, 2002. A generalized geoelectric model of Fennoscandia: a challenging database for long-period 3D modeling studies within the Baltic electromagnetic array research (BEAR) project. Izv. Phys. Solid Earth 38, 855–896.
Veikkolainen, T., Kukkonen, I., Tiira, T., 2017. Heat flow, seismic cut-off depth and thermal modeling of the Fennoscandian Shield. Geophys. J. Int. 211, 1414–1427. https://doi.org/10.1093/gji/ggx373.
Vestøl, O., Ågren, J., Steffen, H., Kierulf, H., Tarasov, L., 2019. NKG2016LU: a new land uplift model for Fennoscandia and the Baltic region. J. Geod. 93, 1759–1779. https://doi.org/10.1007/s00190-019-01280-8.
Vinnik, L., Oreshin, S., Makeyeva, L., Peregoudov, D., Kozlovskaya, E., POLENET/LAPNET Working Group, 2014. Anisotropic lithosphere under the Fennoscandian shield from P receiver functions and SKS waveforms of the POLENET/LAPNET array. Tectonophysics 628, 45–54. https://doi.org/10.1016/j.tecto.2014.04.024.
Warren, J., Hirth, G., 2006. Grain size sensitive deformation mechanisms in naturally deformed peridotites. Earth Planet. Sci. Lett. 248 (1–2), 438–450. https://doi.org/10.1016/j.epsl.2006.06.006.
Weerdesteijn, M.F.M., Conrad, C.P., Naliboff, J.B., 2022. Solid earth uplift due to contemporary ice melt above low-viscosity regions of the upper mantle. Geophys. Res. Lett. 49 https://doi.org/10.1029/2022GL099731 e2022GL099731.
Weerdesteijn, M.F.M., Naliboff, J.B., Conrad, C.P., Reusen, J.M., Steffen, R., Heister, T., Zhang, J., 2023. Modeling viscoelastic solid earth deformation due to ice age and contemporary glacial mass changes in ASPECT. Geochem. Geophys. Geosyst. 24, e2022GC010813 https://doi.org/10.1029/2022GC010813.
Whitehouse, P.L., 2018. Glacial isostatic adjustment modelling: historical perspectives, recent advances, and future directions. Earth Surf. Dynam. 6, 401–429. https://doi.org/10.5194/esurf-6-401-2018.
Whitehouse, P.L., Konstantin, L., Milne, G., Mitrovica, J., Kendall, R., 2006. Impact of 3-D Earth structure on Fennoscandia glacial isostatic adjustment: implications for space-geodetic estimates of present-day crustal deformations. Geophys. Res. Lett. 33, L13502. https://doi.org/10.1029/2006GL026568.
Zhao, N., Hirth, G., Cooper, R., Kruckenberg, S., Cuckjati, J., 2019. Low viscosity of mantle rocks linked to phase boundary sliding. Earth Planet. Sci. Lett. 517, 83–94. https://doi.org/10.1016/j.epsl.2019.04.019.